Analysis of the Longitudinal Spread of Impulsive SEP Events Using Time-Intensity Profiles and Energetic Ion Spectra

Amelia Annarose Lee

Supervised by Dr. Rachael Filwett, Assistant Professor of Physics Montana State University

In partial fulfillment of the

requirements for the Degree of

Bachelor of Arts

May 2024

Department of Physics

Mount Holyoke College

ACKNOWLEDGEMENTS

I first want to thank my thesis committee. Thank you to my research advisor, Professor Rachael Filwett at Montana State University for her unwavering support, patience, and guidance during this process. She has been there at every turn offering not only her expertise but also support and encouragement. I truly would not have been able to do this without her, and I am so grateful to be able to work with her. Thank you to my academic advisor, Professor Spencer Smith. His support has extended far beyond this research, and for that I am so grateful. Although I did not do this research with him, he was always there to ask for updates and listen when aspects of it were not working. Finally, I want to thank Professor Kathy Aidala for all her support. I'm very glad I got to take her electronics class, I enjoyed it, and I learned a lot! Thank you for agreeing to be on my thesis committee, and for reading my thesis!

To my family, thank you for the life-long support, I couldn't have done it without you. To my mom and dad, thank you for always supporting and encouraging my passion and pursuit of science. Thank you for having my back during this process and thank you for letting me talk at you about my research.

I began this research as part of the Montana State University Solar and Space Physics REU program in the summer of 2023. I met wonderful people in my cohort, the organizers of the program, and the researchers and professors I worked with. Thank you for an amazing summer. This research was supported by the NSF Grant No. 1851822.

Finally, this thesis would not have been possible without the incredible support and encouragement from everyone in the Mount Holyoke physics and astronomy community which I am truly grateful to have been a part of.

Thanks to the Integrated Science Investigation of the Sun (IS⊙IS) Science Team (PI: David McComas, Princeton University). This thesis uses EPD data, generated and maintained by the EPD team. Thanks to the Ultra-Low-Energy Isotope Spectrometer (ULEIS) team for use of the ULEIS data. Thanks to the In-Situ Measurement of Particles and CME Transients (IMPACT) team to use of the IMPACT data.

ABSTRACT

Impulsive solar energetic particle (SEP) events occur when protons, electrons, and heavier nuclei are accelerated to high energies (hundreds of MeV) in solar flares and are then observed in interplanetary space. Impulsive SEP events typically last a few minutes to a few hours and have heightened 3He/4He and Fe/O ratios compared to solar wind abundances1. Typically, these events have a longitudinal spread of 20°-40°. However, for unknown reasons, some impulsive events have been observed to have a wide (130°) longitudinal spread. Understanding why some impulsive SEP events are not constrained to a small longitudinal spread or perhaps undergo cross-field diffusion helps us increase our understanding of energetic particle transport and the interplanetary magnetic field configuration.

In this study time-intensity profiles and energetic ion spectra for Helium (Helium-3 and Helium-4 when available), Carbon, Oxygen, and Iron in energy ranges from a few keV to 70 MeV are used to examine the longitudinal spread of six SEP events. These events are April 2-3, 2019, April 4, 2019, April 20-23, 2019, July 11, 2020, July 20, 2020, and May 24-25, 2021, which were previously identified in Mitchell et al. (2023) or Mason et al. (2020). The analysis used four different spacecraft: Parker Solar Probe/IS⊙IS/EPI-Lo, ACE/ULEIS, STEREO-A/IMPACT/LET, and Solar Orbiter/EPD/SIS. We use the findings to discuss the longitudinal spread of heavy ion spectra which show a wide range of longitudinal spreads from event to event.

TABLE OF CONTENTS

LIST OF ILLUSTRATIONS

LIST OF TABLES

Chapter 1

INTRODUCTION

Solar Energetic Particle (SEP) events can greatly affect our local space environment, from our atmosphere to our electrical grids. Understanding how SEP event diffuse and propagate through the interplanetary medium is essential to the prediction of space weather events. This study aims to constrain the longitudinal spread of six different impulsive SEP events using time-series analysis and energetic ion spectra.

This study focused on six solar energetic particle (SEP) events that occurred toward the end of solar cycle 24 and the beginning of solar cycle 25. During all these events, the solar cycle was at a minimum point in its 11-year cycle or rising to a maximum. This cycle corresponds to the number of sunspots observed on the surface of the sun, along with its activity, which can be analogous to the number of solar flares and coronal mass ejections that are observed. This chapter presents an overview of the background physics of impulsive solar energetic particle events and why they are important. In this chapter, I will discuss the origin of impulsive solar energetic particle events, the setup and motivation of this study, and why further study of these events is necessary. Finally, this chapter will go over the types and methods of analysis.

1.1 Solar Energetic Particle (SEP) Events

Origin of Solar Energetic Particle Events

The sun is our most important neighbor. However, despite its proximity to us, a lot of the physical mechanisms on the surface of, and inside of the sun are still poorly understood. For example, the sun's magnetic field is incredibly complicated. It switches polarity every 11 years. The full solar cycle is 22 years, where the sun's magnetic field reverses polarity and then flips back to its original magnetic configuration. As the solar cycle reaches the time when the magnetic field switches polarity, a solar maximum, there is increased radiation which is associated with the increase in activity on the Sun. There is also an increased number of sunspots, coronal loops, and number of large explosive events such as solar flares and coronal mass ejections (CMEs). Furthermore, As the sun rotates, it releases a stream of material, which is known as the solar wind. The solar wind also contains components of the solar magnetic field, that stretch throughout the solar system.

This is sometimes referred to as the interplanetary magnetic field (IMF). Because the sun experiences differential rotation, where the poles of the sun rotate more slowly than the equator of the sun, the open magnetic field lines and material released from the sun twist into an Archimedean spiral as it extends through the solar system (pictured in Figure 1.1). This is known as the Parker Spiral after Eugene Parker who proposed the existence of the solar wind in 1960 (Parker 1958).

Figure 1.1: An artist's rendition of the Parker Spiral. (Wikipedia, Werner Neil NASA)

Solar energetic particle events are associated with solar eruptions like solar flares or coronal mass ejections (CMEs). Solar flares are eruptions of electromagnetic radiation originating in the Sun's atmosphere which spatially correspond with active regions or sunspots. They occur from a rapid release of energy stored in the sun's magnetic field and occur with more frequency at solar maximums (Fletcher et al. 2011). Although the most widely accepted hypothesis is that solar flares and particle acceleration occur due to magnetic reconnection (Reames 2023), the origin and prediction of solar flares is still an active area of research. The duration of solar flares are short compared to the duration of CMEs (minutes to hours) but can release 10^{23} ergs of energy (Fletcher et al. 2011). Solar flares emit radiation across the entire electromagnetic spectrum and are associated with radio bursts and solar energetic particle acceleration (Fletcher et al. 2011). Finally, Gosling (1993) mentions that although solar flares are often associated with CMEs, there is no accepted theoretical connection.

Coronal Mass ejections (CMEs) are massive solar eruptions that occur from a large-scale ejection of the coronal magnetic field and plasma contained within it (Malandraki and Crosby 2018). According to Malandraki and Crosby (2018), the

observational definition of a CME is an extended white light feature on a coronagraph traveling outward from the sun. CMEs are larger and more structured compared to solar flares. While solar flares last minutes to hours, CMEs can last for days (Malandraki and Crosby 2018).

Solar Energetic Particle (SEP) Events

Solar flares are made up of mainly electrons and protons. However, the focus of this study is the behavior of ions and heavy ions in particular (He and heavier). The protons, electrons, and heavier nuclei (helium, iron, oxygen, etc.) accelerated by these events and observed in interplanetary space are referred to as solar energetic particle events. These particles are accelerated from background solar wind energy levels (keV, or lower) to relativistic energies (GeV) in some cases (Malandraki and Crosby 2018).

There are two categories of events, although the lines between the classifications are often blurry. Impulsive SEP events are associated with solar flares, last on time scales of minutes to hours, have a ^{3}He rich particle population, and heightened type III radio bursts. ^{3}He is an isotope of helium with 2 protons and 1 neutron. As such, these events are often referred to as ^{3}He-rich events. Additionally, particles in impulsive SEP events are accelerated at the flaring site in the lower atmosphere of the sun (Malandraki and Crosby 2018). Gradual SEP are often associated with CMEs, last on time scales of hours to days, and are associated with type II radio bursts. Unlike impulsive events, particles from gradual events are often accelerated by shock waves associated with CMEs. These shock waves are generated by CMEs that travel faster than the background solar wind speed (400 km/s). As a consequence of the additional particle acceleration as well as the size of the CMEs, gradual events typically have broad latitudinal and longitudinal spreads that can reach over 90 degrees (Desai and Giacalone 2016). Figure 1.2 illustrates a gradual event vs. an impulsive event. Particles from an impulsive event (panel b) are accelerated in the lower atmosphere of the sun and travel down IMF lines magnetically connected to the active region (Malandraki and Crosby 2018).

This study concerns impulsive or ^{3}He- rich events. ^{3}He- rich events are associated with solar flares and ^{3}He- rich particle populations. It is important to note that these events are defined by the particle population and duration, not by the type of eruption the event originated from. There are often simultaneous events on the sun that can lead to the mixing of different particle populations. Some events can be

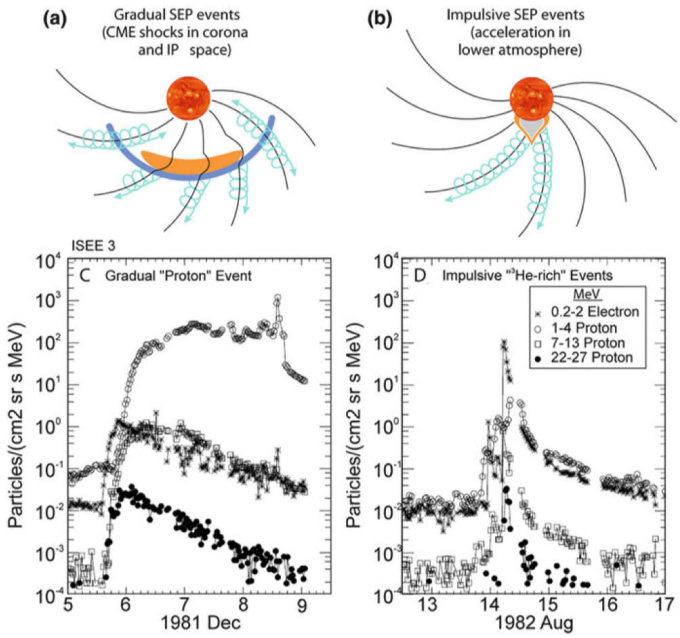

Figure 1.2: Gradual vs. Impulsive SEP event. The particles in an impulsive SEP event are accelerated in the lower atmosphere of the sun and travel down IMF lines connected to flare site (Reproduction from Desai and Giacalone (2016) as cited in Malandraki and Crosby (2018)).

a combination of gradual and impulsive and have characteristics of both types of events. Impulsive events have a short duration compared to gradual events and often exhibit a large sharp spike in time series data at the time of the onset of the fare (Malandraki and Crosby 2018). Panel C in Figure 1.2 illustrates the sharp spike at the onset of the flare. As mentioned earlier, these events are also characterized by an enhancement in ^{3}He leading to ^{3}He/^{4}He ratios that can be enhanced by a factor of 1,000 compared to the background solar wind ratio (5x10-4) (Reames 2021, Mewaldt et al. 2008). According to Reames (2021), the ^{3}He/^{4}He ratio in impulsive SEP events is often greater than one. There is also an increase in the Fe/O ratios. Recent studies suggest that ^{3}He rich events correlate directly to solar flares due to the fundamental physics of magnetic reconnection in solar flares (Reames 2023). High enough enhancements in these ratios are good indicators of an impulsive event. The particles accelerated in an impulsive SEP are “shot out” (accelerated) from the flare site, in the lower atmosphere of the sun (Malandraki and Crosby 2018). The longitudinal spread of an SEP event refers to how wide particles from SEP events spread out horizontally. Because the beginning of the particle’s journey is in the lower atmosphere of the sun, the particles travel on IMF lines well connected to

the flare site. This means that usually, the longitudinal spread of these events is relatively narrow > 60 degrees (Wiedenbeck et al. 2012). However, some studies report large longitudinal spreads (136 degrees) in ^{3}He- rich events (Wiedenbeck et al. 2012).

Longitudinal Spread and Cross-Field Diffusion

The longitudinal spread of an SEP event is contributed to by radial and cross-field diffusion. Radial or parallel diffusion occurs as particles with different energies and different speeds travel from the flare site out into interplanetary space, along IMF lines. Particle fluxes at a spacecraft located closer to the sun will be higher than particle fluxes at a spacecraft located at 1 AU. Part of the overall longitudinal spread comes from cross-field or perpendicular diffusion. Cross-field diffusion occurs when SEPs travel across (perpendicular to) the interplanetary magnetic field instead of traveling along an IMF line connected to the flare site. The amount of cross-field diffusion can be indicated by the cross-field diffusion coefficient which quantifies how far an energetic particle deviates from the ambient magnetic field (Laitinen et al. 2013). Laitinen et al. (2013) defines the cross-field diffusion coefficient in terms of the average variance of particles and time where σ is the average variance of particles and t is time $K_{\perp,i} = \sigma_i^2(z,t)/2t$. The cross-field diffusion coefficient is calculated using models such as iPath and AWSoM (Li et al. 2020).

In most plasmas, the ambient magnetic field sets a direction, and random or turbulent field components induce cross-field transport (Costa et al. 2013). In the case of energetic particles, the direction set by the magnetic field should follow the Parker Spiral. However, in reality, the Parker Spiral is a good approximation of the background field, but it becomes extremely complicated when other mechanisms of the sun are involved. Furthermore, the cross-field diffusion coefficient can also evolve temporally. According to Laitinen et al. (2013), early in an event the cross-field diffusion coefficient may be smaller because particles remain on initial interplanetary magnetic field lines. Later in the event the cross-field diffusion coefficient may become larger. Although calculating the cross-field diffusion coefficient was not in the scope of this thesis, if this study continues, calculating the cross-field diffusion coefficient would be the next step in the analysis.

1.2 Study Construction and Motivation

Several studies have looked at how SEP events longitudinally spread with cross-field diffusion or without cross-field diffusion. These studies concluded that cross-field

diffusion occurs, but the circumstances under which there is more or less diffusion is not understood. The reason why rates of diffusion are different is also not understood. This is one of the motivators of our study. Quantifying the longitudinal spread of more events will help us to understand which events experience a lot or a little cross-field diffusion. Additionally, because impulsive events are often smaller and less energetic than gradual events, and are mainly made up of protons and electrons, not many studies of impulsive events employ multiple spacecraft and heavy ions. This study provides insights to the longitudinal spread of these events and diffusion of heavy ions occurring in impulsive SEP events from a multi-spacecraft and heavy ion perspective.

Additionally, space weather can have a large impact on our technology and atmosphere. 164 years ago, from September 1-2 1859, particles from a massive solar flare CME combo hit the Earth. It caused the most intense geomagnetic storm in recorded history (Tsurutani et al. 2003). Strong auroral displays were reported globally, and in the United States, the aurora was reported as far south as the Colorado Rocky Mountains. It was so strong it caused fires in telegraph stations. This event was observed by Richard Christopher Carrington, so this geomagnetic storm is referred to as the Carrington Event. Geomagnetic storms are temporary disturbances in the Earth's magnetic field and are caused by or associated with many solar phenomena including SEP events. These events are unpredictable, specifically events with a sharp peak on a short time scale. High-energy SEPs of all types have been observed to have harmful effects on space systems, avionics, and even humans (Malandraki and Crosby 2018). Understanding and mitigating effects of SEP events is an important part of risk assessment and management of space systems and ground electronics systems. Another event on the scale of the Carrington Event would likely cause widespread blackouts and GPS failure. It is increasingly important to understand the mechanisms behind diffusion in SEP events, so space weather events can be better understood, and measures can be taken to prevent harm to GPS, electrical grid, and space instruments.

This study uses four different spacecraft to study six different impulsive SEP events. The basis for this study is Mitchell et al. (2023) which identifies 138 SEP events using the Parker Solar Probe's (PSP) Integrated Science Investigation of the Sun (IS$\odot$IS) instrument suite. These events are a mix of impulsive, gradual, and mixed events. The IS$\odot$IS instrument suite contains two instruments, EPI-Hi and EPI-Lo, which combined cover a total energy range of about 20 keV to 200 MeV (Michell et

al. 2023). The events in our study were initially identified using this paper. After the events were identified, particle data from other spacecraft with similar energy ranges was used to look for signs of the events. The other spacecraft used in this study were Solar Orbiter's (SolO) Energetic Particle Detector (EPD) instrument suite, specifically the Suprathermal Ion Spectrograph (SIS), the Advanced Composition Explorer's (ACE) Ultra-Low Energy Isotope Spectrometer (ULEIS), and the Solar Terrestrial Relations Observatory- Ahead's (STEREO-A) In situ Measurements of Particles And CME Transients (IMPACT) instrument suite, specifically the Low Energy Telescope (LET). Then, based on the angular separation of the spacecraft, and which spacecraft saw what event, we are able to constrain the longitudinal spread of each event.

1.3 Event Selection

Six impulsive solar energetic particle events were studied using data from four different spacecrafts. These events are: April 2-3, 2019, April 4, 2019, April 20-23, 2019, July 11, 2020, July 20, 2020, and May 24-25, 2021. The events are referred to as Event 1 to Event 6 in order of occurrence. Mitchell et al. (2023) presents a living catalog of SEP and stream interaction (SIR) events identified by the Parker Solar Probe, as well as event identification methodology, and highlights of several events.

Events 1- 3 and Event 6 were identified by the Parker Solar Probe in Mitchell et al. (2023). As the first three events occurred before Solar Orbiter launched, analysis for Events 1 through 3 will not include data from Solar Orbiter. The other two events (Events 4-5) were identified by Solar Orbiter in Mason et al. (2020). With the exception of Event 5 (July 20, 2020), the events identified by Solar Orbiter were also identified by the Parker Solar Probe in Mitchell et al. (2023) and other studies (Wiedenbeck et al. 2020 and McComas et al. 2019). There is a more comprehensive online spreadsheet of the events recorded by Mitchell et al. (2023).

1.4 Measurements

Two types of analysis were done with these data, energetic ion spectral analysis and time-series analysis. Time series analysis is the main type of analysis done in this project. It gives us an indication of if each spacecraft saw each event, and what the ion fluxes look, how much of each ion is present in the event. There is a lot of basic information contained in this analysis, primarily the onset and peak times and duration of the event, which is particularly important when occurring

the time onset at each spacecraft. It also gives a good indication to the maximum energies that the particles are accelerated to. Time series analysis can also give an indication of the longitudinal spread for each event (if multiple spacecrafts pick up one event, then the longitudinal spread was wide enough for the events to be picked up by multiple spacecrafts), what particle seed populations were like at the onset of the event, how particles are being accelerated, and even if there may be cross-field diffusion occurring. One product of time series analysis is plots called time-intensity profiles. These plots plot the flux (on a log scale) on the y-axis and time over the event on the x-axis. The flux is summed across the entire energy range to show general trends over the entire energy range. Panels (C and D) in Figure 1.2 on page 4 show time-intensity profiles over smaller energy ranges for a gradual and an impulsive event. Impulsive events exhibit a sharp spike in flux at the onset of an event, and fall off quickly as the event finishes, while gradual events exhibit a sharp peak at the onset of an event but fall off more slowly.

The second type of analysis done was the energetic ion spectral analysis. Energetic ion spectra provide another angle of analysis for SEP events. All of the spacecraft record particle flux by sorting each particle into a specific energy bin at a specific time. The spectra shows the fluence (flux integrated over time), versus the energy, which is recorded as the average energy of the energy bin. This gives a view of the event that is separated from time, and makes it easier to analyze changes in particle fluence as a function of the energy. The spectra also indicate how the particles are being accelerated out of the flare. For example, if there is an evolution of the spectra from spacecraft to spacecraft, this indicates a possible longitudinal gradient or radial transport effect. The change in total fluence with respect to energy of particles in solar energetic particle events are proportional to a power-law

$$dJ/dE \propto E^{-\gamma}$$

. The spectra index (γ) is calculated by computationally fitting the spectra to an Ellison- Ramaty equation (Liu et al. 2020, Bruno et al. 2017). In this study, the equation used was

$$J = J_0 E^{-\gamma} e^{\frac{E}{E_0}}$$

, where gamma is the spectral index, J0 is a constant and E0 is the cutoff energy (Liu et al. 2020). This is typically analyzed on a log-log scale.

Chapter 2

SPACECRAFTS, INSTRUMENTATION, AND DATA PRODUCTS

This study uses data from four different spacecraft, and a minimum of one instrument on each. As discussed in Chapter One, these data are from the Parker Solar Probe (PSP), the Advanced Composition Explorer (ACE), the Solar Terrestrial Relations Observatory- Ahead (STEREO-A), and Solar Orbiter (SolO). Each spacecraft is equipped with one or more energetic particle detectors covering the energy range from a few keV to multiple MeV, the range of interest of this study. Each energetic particle detector records variations in time, and energy, typically for multiple ion species. In addition to energetic particle detectors, the magnetic field strength was measured using the onboard magnetometers for each spacecraft. This chapter provides a comprehensive review of the spacecraft and instruments utilized including their energy range, time and energy resolution, and resulting data products.

2.1 Parker Solar Probe/IS⊙IS (EPI-Hi, EPI-Lo)

Parker Solar Probe (PSP, pictured in Figure 2.1) will be the first spacecraft to travel within four million miles of the sun. Parker Solar Probe's purpose is to provide a statistical survey of the outer corona, and has three main science objectives: to trace the flow of energy that heats and accelerates the solar corona and solar wind, to determine the structure and dynamics of the plasma, and magnetic fields at the sources of the solar wind, and to explore the mechanisms that accelerate and transport energetic particles (NASA Parker Solar Probe Mission).

The scientific objectives associated with the PSP mission will help us to understand the long-term problem of coronal heat. Progress toward meeting these objectives will significantly increase our ability to forecast space weather events that impact Earth, particularly the third objective of understanding the acceleration and transport of energetic particles, which motivates this study.

PSP will make 24 orbits in its nominal mission, and is currently in orbit 18. It uses seven Venus gravity assists to lower the perihelion of the orbit.The orbit is highly elliptical, and each orbit will take PSP closer to the Sun. On the final three orbits, PSP will come within nine solar radii or almost four million miles of the sun (NASA Parker Solar Probe Mission). This distance allows the mission to sample the young

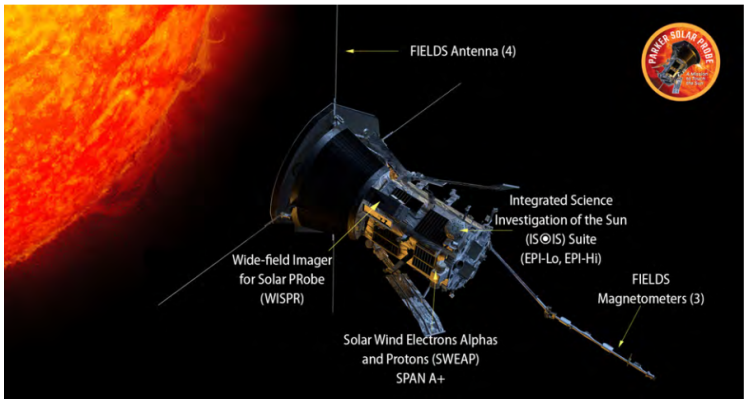

Figure 2.1: Parker Solar Probe with several instruments labeled (NASA/Johns Hopkins APL/Margaret Brown as credited in PSP Press Kit).

solar wind by flying through the upper atmosphere of the sun.

Integrated Science Investigation of the Sun (IS⊙IS) Instrument Suite

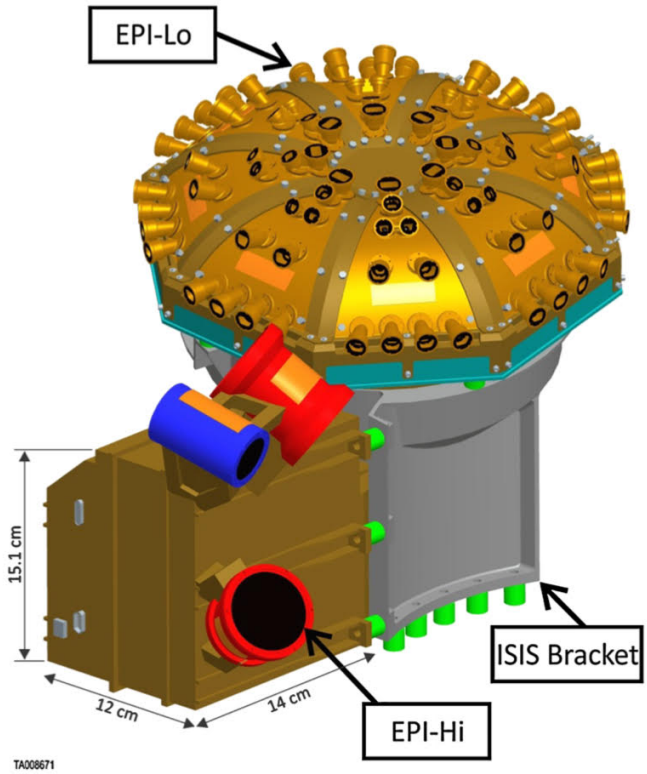

Figure 2.2: IS⊙IS Instrument Suite, EPI-Hi and EPI-Lo (McComas et al. 2014).

The IS⊙IS instrument suite (pictured in Figure 2.2) is designed to explore the mechanisms that produce, accelerate, and transport SEPs in the heliosphere (McComas

et al. 2014). It uses two complementary instruments to make measurements; the Energetic Particle Instrument- High Energy (EPI-Hi) and the Energetic Particle Instrument- Low Energy (EPI-Lo) which have a combined energy range of 20 keV/nuc to 200 MeV/nuc (McComas et al. 2014).

EPI-Lo is a time-of-flight (TOF) mass spectrometer. It uses the principle that ions with the same charge but different masses travel at different speeds in magnetic fields. EPI-Lo, pictured in Figure 2.3, measures energetic electrons from 25-1000 keV/nuc and ions over 20 keV/nuc- 20 MeV/nuc, which is the lower portion of the IS⊙IS energy range. It is made up of eight sensor wedges with 10 apertures per wedge (referred to as look directions) on each wedge so that it can sample a 2π steradian field of view (Mitchell et al. 2023).

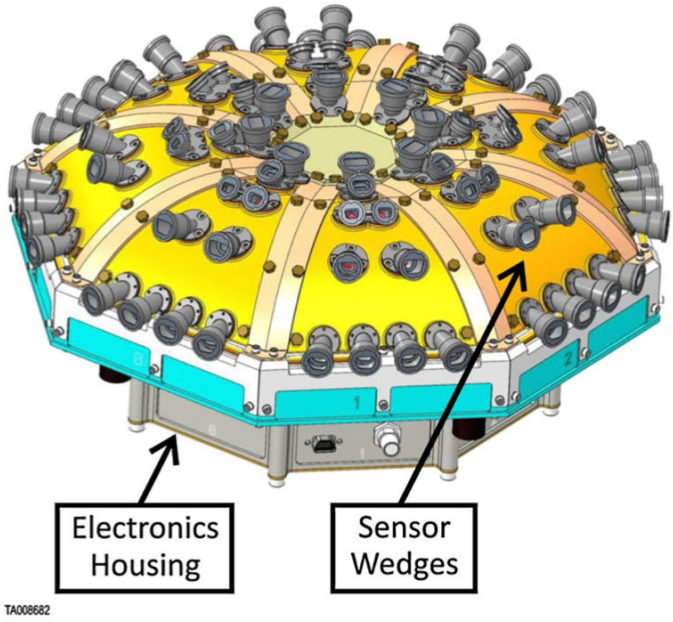

Figure 2.3: EPI-Lo Mechanical design (McComas et al. 2014).

The sensor portion of the instrument is mounted above the electronics box (McComas et al. 2014). Energy resolution describes the ability of an instrument to differentiate two ions with different kinetic energies. EPI-Lo has an energy resolution of 11%. Ion-mass resolution describes the ability of EPI-Lo to distinguish between ions of different masses. The ion-mass resolution has to be high enough to distinguish between all the ion species studied on the PSP mission which are Hydrogen, Helium-3, Helium-4, Carbon, Oxygen, Neon, Magnesium, Silicon, and Iron. Each ion is

detected within a slightly different energy range. The majority of EPI-Lo data has a five-minute minute integration time, although rate data for ions are generated between 30 and 5 seconds (McComas et al. 2014, McComas et al. 2023). Finally, to manage power and large data quantities, PSP periodically turns off to send data back to Earth. During data downlink periods, PSP will transmit data every day anywhere from 10 hours to 24 hours a day. Otherwise, PSP communicates with Earth three times a week (MASA PSP Press Kit).

The EPI-Lo team publishes data in CDF files, a file format that is standard to many NASA heliophysics missions. These data products include count-rate, flux, and error for all ions and electrons. The files also include data such as energy, time, latitude etc. Because EPI-Lo has 80 apertures, within the CDF file, flux data takes the form of a 3D array: [epoch, look-direction, energy bin]. In the analysis of these data, the arrays were summed along the look-direction axis, which is standard when not analyzing direction-dependent features. The energy range for flux and count rate data for each element are binned into 21-44 intervals and are taken at several cadences. The flux data used in this study were the 60-second cadence (Poduval et al. 2024).

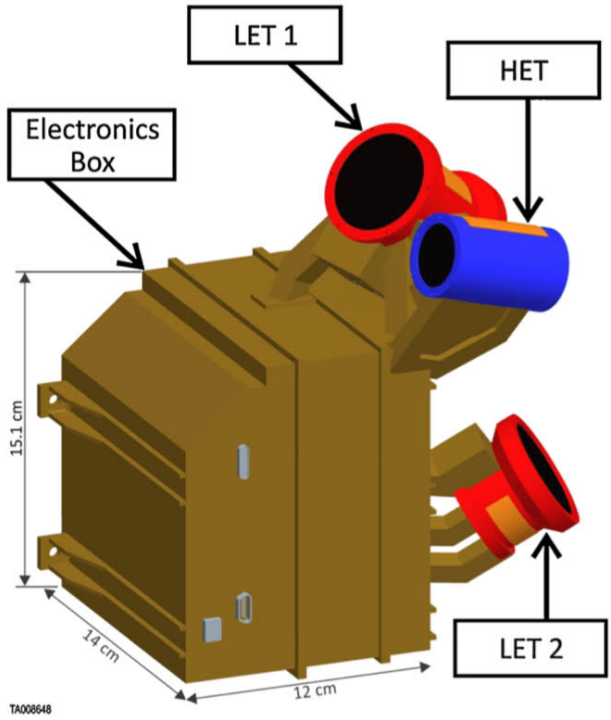

Figure 2.4: EPI-Hi Mechanical design (McComas et al. 2014).

The other instrument in the IS⊙IS suite is the Energetic Particle Instrument- High Energy (EPI-Hi), pictured in Figure 2.4. EPI-Hi is made up of two telescopes, High Energy Telescope (HET) and Low Energy Telescope (LET). There are two LET telescopes aboard EPI-Hi: LET1 and LET2. LET1 faces the sun and LET faces away from the sun. LET data from EPI-Hi was used in this study. EPI-Hi measures protons, electrons, and heavy ions in the MeV range (McComas et al. 2014). HET and LET have different but overlapping energy ranges. LET measures protons and heavy ions from 1 to 20 MeV/nuc, and HET measures protons and heavy ions to at least 100 MeV/nuc (McComas et al. 2014). Figure 2.5 is a plot of the energy range of each ion measured by EPI-Hi. In addition to the three telescopes, EPI-Hi also contains the data processing unit responsible for controlling the instrument and communicating with Earth.

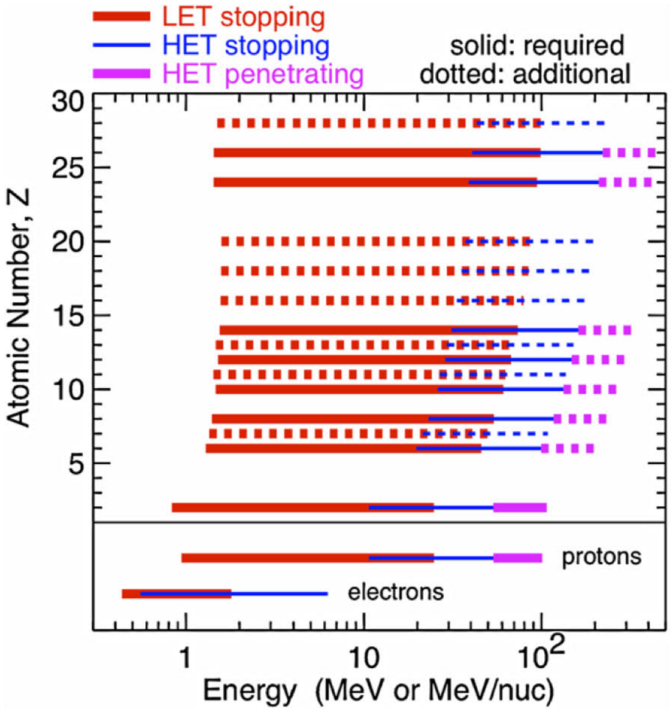

Figure 2.5: Plot EPI-Hi Ion Energy Range, atomic number (Z) vs. MeV/nuc (McComas et al. 2014).

EPI-Hi measures the electrons, protons, and heavy ions using the dE/dx versus total energy technique based on ion-implanted silicon SSDs (McComas et al. 2014). This describes a technique to distinguish between ions in an SSD. The derivative dE/dx describes energy loss per unit length. As the ion passes through the detector, the loss of energy is calculated then used to identify the ion (Mewaldt et al. 2008). EPI-hi

has a variety of cadences. Data used in this study is the 3600 cadence data. Like EPI-Lo, the EPI-Hi team publishes data in a CDF file. Because EPI-Hi data from each telescope is published in seperate CDF files, the data structures are simpler.

2.2 STEREO-A/IMPACT (LET)

The STEREO mission, or the Solar TErrestrial RElations Observatory are two space based observatories, STEREO-A (Ahead) and STEREO-B (Behind). STEREO-A and STEREO-B are two nearly identical spacecraft that orbit the sun just inside one astronomical unit. STEREO is the third mission in NASA's Solar Terrestrial Probes program. STEREO-A and STEREO-B were launched in December 2006 with STEREO-A moving ahead of Earth, and STEREO-B moving behind Earth (NASA STEREO, Mewaldt et al. 2008). Unfortunately, STEREO-B lost contact with Earth in 2016.

Like the Parker Solar Probe, STEREO's purpose is to study the sun. The main goal of the mission was to provide the first stereoscopic measurements to study the sun and the nature of CMEs (NASA STEREO). The more specific mission objectives are to understand the causes and mechanisms of CMEs, to characterize the propagation of CMEs through the heliosphere, to learn about the mechanisms and sites of energetic particle acceleration in the corona and the interplanetary medium, and to improve the determination of the structure of the ambient solar wind (NASA STEREO). STEREO-A is pictured in Figure 2.6.

Because NASA lost contact with STEREO-B before the SEP events studied in this project occurred, only data from STEREO-A was used in this study. STEREO-A consists of four instrument suites. The first instrument is the Sun-Earth Connection Coronal and Heliospheric Investigation (SECCHI) which is four instruments, an EUV imager, an inner and outer coronagraph, and a heliospheric imager. The second instrument suite is STEREO/WAVES (SWAVES) which is an interplanetary radio burst tracker. The third instrument suite is the In-Situ Measurement of Particles and CME Transients (IMPACT) which is a suite of seven instruments that sample the distribution of solar wind plasma electrons and the characteristics of SEP ions and electrons. Finally, Plasma and Suprathermal Ion Composition (PLASTIC) measures the solar wind and measures characteristics of protons, alpha particles, and heavy ions (NASA STEREO).

Figure 2.6: STEREO-A (NASA/Johns Hopkins University Applied Physics Laboratory as cited on Wikipedia).

IMPACT (LET)

IMPACT is the instrument suite on STEREO-A (and B) that is dedicated to the study of SEPs (pictured in Figure 2.7). IMPACT has four energetic particle detectors, and seven instruments in total. The energetic particle detectors including the Low Energy Telescope (LET). The other energetic particle detectors include a high energy telescope (HET), a suprathermal ion telescope (SIT) and a solar electron and proton telescope (SEPT). IMPACT's energetic particle detector's main science objective is to discover the mechanisms and sites of energetic particle acceleration in the low corona and interplanetary medium (Mewaldt et al. 2008).

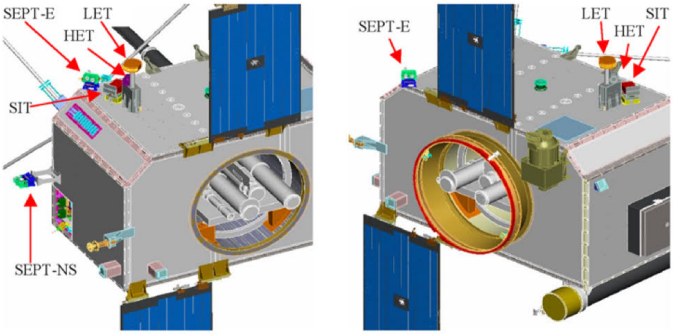

Figure 2.7: IMPACT Suite with LET labeled (Mewaldt et al. 2008).

LET is one of the four energetic particle detectors in the IMPACT suite. All the instruments in the IMPACT suite covers an energy range from 0.03 to 100 MeV for ions and electrons from 0.03 to 6 MeV. LET is a double fan arrangement of 14 solid state detectors (SSDs) that cover an energy range from 1.5 to 70 MeV. Figure 2.8 plots the energy range of all ions distinguished by LET (Mewaldt et al. 2008).

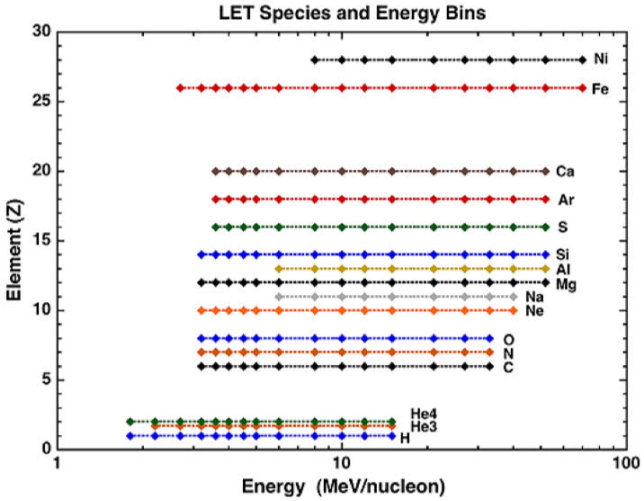

Figure 2.8: LET energy range, atomic number (Z) Vs. energy (MeV/nuc) (Mewaldt et al. 2008).

LET has the ^{4}He mass resolution of 0.23 amu, meaning it has the capability of resolving between ions with a mass difference greater than or equal to 0.23 amu (Mewaldt et al. 2008). It can resolve Hydrogen, Helium, Carbon, Nitrogen, Oxygen, Neon, Sodium, Magnesium, Aluminum, Silicon, Sulfur, Argon, Calcium, Iron, and Nickel (Mewaldt et al. 2008). Although the mass resolution would allow LET to distinguish between ^{3}He and ^{4}He, data files for ^{3}He and ^{4}He are filled with the filler value for bad or missing data, so the unresolved Helium data was used. The energy range for flux data for each element is binned into 10-15 intervals. For example, the energy range for Helium is 2.2-15 MeV/nuc, and the first energy bin for Helium is 2.2-2.7 MeV/nuc (Mewaldt et al. 2008). LET data is available in one-minute, 10-minute, 1-hour, daily, and 27-day averages. The LET data used in this study are the 10-minute averages. The LET team publishes the data as a text file that includes flux, count rate, and uncertainty data as well as the year, day of year, hour of day, minute of hour, second of minute, and LET live time.

2.3 ACE/ULEIS

ACE, or the Advanced Composition Explorer is the third spacecraft used in this study. It was launched on August 25, 1997, and orbits the first Lagrange point (typically referred to as L1), about 1 Au from the sun. Originally the mission had a life expectancy of five years, but has since far exceeded it (ACE launched in 1997). ACE's main objective is to measure and compare particle samples from the solar wind to cosmic rays (NASA ACE). Its specific science goals pertaining to solar energetic particles include making direct measurements of charge and mass-dependent fractionation during SEP events, constraining solar flare and coronal and interplanetary shock acceleration models, and testing theoretical models for 3He-flare flares and solar gamma-ray events (NASA ACE). ACE is pictured below in Figure 2.9.

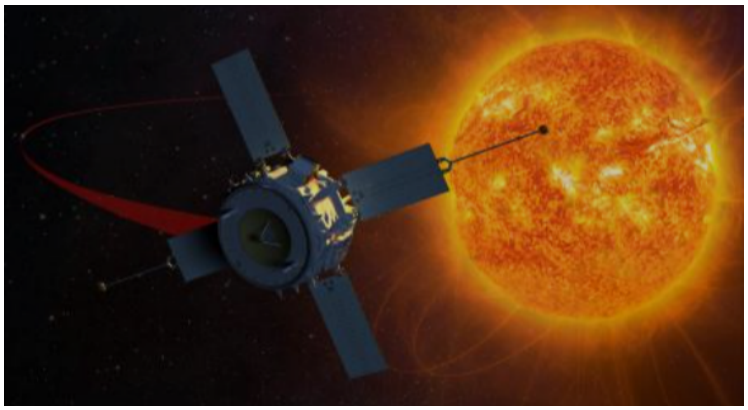

Figure 2.9: The ACE Spacecraft (ACE APL webpage).

ACE has nine instrument suites. The Cosmic Ray Isotope Spectrometer (CRIS), measures energetic particles over the highest portion of the ACE energy range. The Electron Proton Alpha Monitor (EPAM) is an energetic particle detector that covers a lower portion of the energy range. The Magnetometer (MAG) measures the strength of the magnetic field. The Real Time Solar Wind (RTSW) monitors the solar wind and provides warnings for geomagnetic storms. The Solar Energetic Particle Ionic Charge Analyzer (SEPICA) determines the ionic charge states of particles. The Solar Isotope Spectrometer (SIS) is another energetic particle detector that covers a middle portion of the ACE energy range. The Solar Wind Electron, Proton and Alpha Monitor (SWEPAM) provides solar wind observations. The Solar Wind Ion Composition Spectrometer (SWICS) and the Solar Wind Ion Mass Spectrometer (SWIMS) measure the composition of the solar wind. Finally, the Ultra-Low-Energy Isotope Spectrometer (ULEIS) is an energetic particle detector that covers

the lower-middle portion of the ACE energy range (NASA ACE). It is the main instrument used in this study. It is important to note that due to the long-lived nature of ACE some of the instruments are no longer functional, or have had to undergo gain corrections over the years.

Ultra-Low Energy Isotope Spectrometer (ULEIS)

ULEIS is one of the four mass spectrometers on ACE. In total, the mass spectrometers aboard ACE cover an energy range from 1 keV/ nuc (solar wind energy) to 1000 MeV/nuc (galactic cosmic ray energy). ULEIS covers an energy range from 45 keV/nuc to a few MeV/nuc (Mason et al. 1998).

Like the Parker Solar Probe, ULEIS (pictured below in Figure 2.10) uses the time-of-flight principle to determine the mass of the ion, however it only has one aperture.

Figure 2.10: ULEIS Instrument (Mason et al. 1998).

ULEIS has a goal mass resolution of less than 0.15 amu for Z = 6 and 0.5 for Z=26. It can resolve hydrogen, helium-3, helium-4, carbon, oxygen, neon, and iron (Mason et al. 1998). Like PSP/ISOIS (EPI-Lo) and STEREO-A/IMPACT (LET), ACE/ULEIS the energy range for flux data are binned into several passbands. ULEIS has two channel designations that both separate fluxes into passbands covering the energy range. The amount of bins ranges over species and channel, but ranges between 2 bins to 12 bins (Mason et al. 1998). For example, hydrogen has five bins to cover an energy range of 0.16 MeV/nuc to 7.24 MeV/nuc while 4He has 15 bins to cover an energy range of 0.063 MeV/nuc to 8.67 MeV/nuc. Additionally, the cadence

these data were measured at was one hour. This study uses the one-hour averages. The ULEIS team publishes the data in a text file. The text file includes flux and uncertainty data as well as the year, day, and Epoch.

2.4 Solar Orbiter/EPD (SIS)

Solar Orbiter (SolO) is a solar probe launched by the European Space Agency in Feburary of 2020. It's main objective is to perform close up and high-resolution studies of the sun and inner heliosphere (European Space Agency Solar Orbiter Overview). It will be the first spacecraft to provide close-up and high-resolution images of high latitude regions on the sun that are difficult to see from Earth. The Solar Orbiter mission has four science objectives: to the origin of the solar wind and the coronal magnetic field, to identify how solar transients drive heliospheric variability, to identify how solar eruptions produce energetic particle radiation, and to identify how and what drives connections between the sun and the heliosphere (European Space Agency Solar Orbiter Overview). Solar Orbiter is pictured in Figure 2.11.

Figure 2.11: Solar Orbiter (NASA's Goddard Space Flight Center Conceptual Image Lab as cited on Wikipedia).

The Solar Orbiter and the Parker Solar Probe are the two spacecraft in this study that actually approach the sun. Although SolO will not get as close to the sun as the PSP, it will get within 60 solar radii of the sun (European Space Agency Solar Orbiter Overview). By using a combination of gravity assists from Venus and Earth, SolO will reach its perihelion every six months. The Venus gravity assists will also increase the inclination of Solar Orbiter's orbit so that the polar regions of the sun (at an angle greater than 30 degrees) can be imaged (European Space Agency Solar Orbiter Overview).

Solar Orbiter has 10 instrument suites. The energetic particle detector suite (EPD) measures energetic particles around the spacecraft. The magnetometer (MAG) measures the magnetic field around the spacecraft. The radio and plasma wave sensors (RPW) measure variations in the magnetic fields. The solar wind plasma analyser (SWPA) is a suite of instruments that will measure various properties of the solar wind. There are two solar corona imagers, Metis takes images of the corona in visible and UV light, and the extreme ultraviolet imager (EUI) images the chromosphere. The polarimetric and helioseismic imager (PHI) provides measurements of the magnetic field across the photosphere. The heliospheric imager (SoloHI) takes images of the solar wind. Finally, there is a spectral imager (SPICE), and an X-ray spectrometer (STIX) (European Space Agency Solar Orbiter Instruments).

Energetic Particle Detector/Suprathermal Ion Spectrograph (EPD/SIS)

The Energetic Particle Detector is a suite of instruments that measure the spectra, composition, time variation, and directional distribution of solar energetic particles (Rodríguez-Pacheco et al. 2020). EPD aims to answer the third science objective of the SolO mission: how do solar eruptions produce energetic particle radiation that fills the heliosphere. EPD has three more specific objectives- to identify where and how energetic particles are injected, as well as what particles make up the seed populations, to identify acceleration mechanisms, and finally to identify transport mechanisms (Rodríguez-Pacheco et al. 2020). The EPD consists of four detectors, a suprathermal electron and proton detector (STEP), an electron and proton telescope (EPT), a suprathermal ion spectrograph (SIS), a high energy telescope (HET), and an instrument control unit (Rodríguez-Pacheco et al. 2020). The EPD instrument suite covers an energy range from a few keV/nuc to 450 MeV/nuc. EPD is pictured in Figure 2.12.

The suprathermal ion spectrograph (SIS) is a time-of-flight mass spectrometer that covers an energy range from 14 keV/nuc to 20.5 MeV/nuc and resolves ions with atomic numbers from 2-26 (Rodríguez-Pacheco et al. 2020). SIS has two fields of view, one sunward (referred to as SIS-A) and one anti-sunward (referred to as SIS-B). The data used in this study were the sunward field of view (SIS-A). Figure 2.13 plots the energy range of all ions distinguished by SIS.

SIS measures fluxes at three different cadences, slow, medium, and fast. The slow data is taken at a cadence of 1800 seconds (30 minutes), the medium data is taken at a cadence of 30 seconds, and the fast data is taken at a cadence of 3 seconds

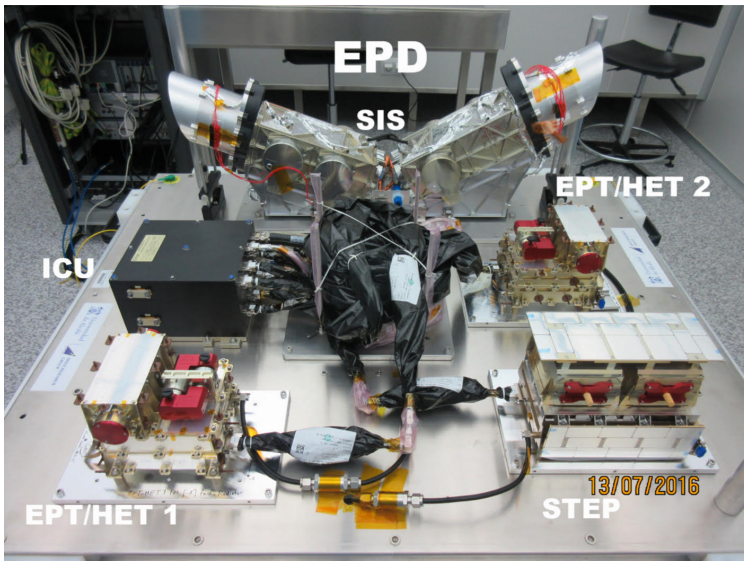

Figure 2.12: EPD with SIS labeled (Espinosa 2022).

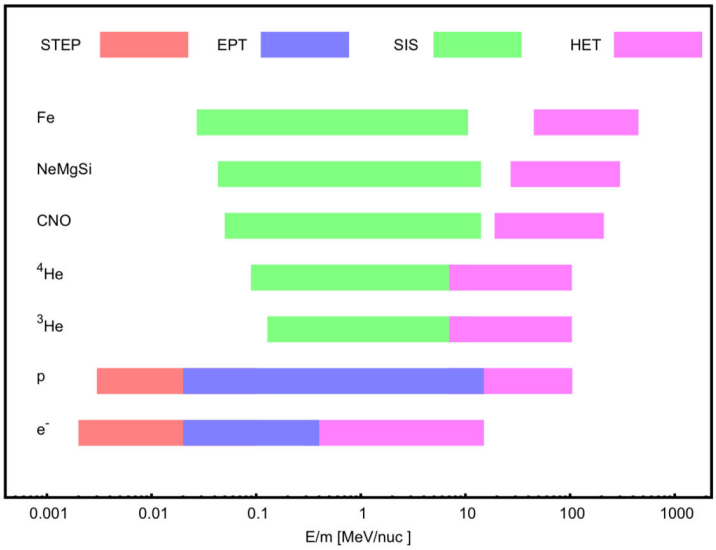

Figure 2.13: EPD Ion Energy Range: Ion Vs. energy (MeV/nuc)(Espinosa 2022).

(Espinosa 2022). This study uses the medium (30 second) cadence data. Like the other spacecraft, the energy range for the flux data is binned into several passbands depending on the species, with 11-17 bins. For example, the flux data for iron has 15 bins to cover an energy range of 0.05 MeV/nuc to 10 MeV/nuc (Espinosa 2022). The SIS team publishes the flux data as a CDF file that includes flux, uncertainty, and epoch (time) data, as well as the width of the energy passbands for each species, the lowest measured energy in each passband, and a text description for each energy

bin (Espinosa 2022).

Chapter 3

EVENTS

Six SEP events are identified in Mason et al. (2020), Mitchell et al. (2023), McComas et al. (2019), and Wiedenbeck et al. (2020). These Events are April 2-3, 2019, April 4, 2019 (identified in Mitchell et al. 2023, McComas et al. 2019, and Wiedenbeck et al. 2020), April 20-23, 2019 (identified in Mitchell et al. 2023 and Wiedenbeck et al. 2020)), July 11, 2020 (identified in Mason et al. 2020 and Mitchell et al. 2023), July 20, 2020 (identified in Mason et al. 2020), and May 24-25, 2021 (Identified in Mason et al. 2020 and Mitchell et al. 2023). The events are referred to as events 1-6 in order of occurrence and are spread over three years, three in 2019, two in 2020, and one in 2021.

3.1 Event 1: April 2-3, 2019

The first event occurred from April 2-3, 2019. It was identified by the Parker Solar Probe in Mitchell et al., (2023). Below, in Table 3.1, are the distance from the sun, the start Carrington longitude, and the end Carrington longitude of each of the spacecraft during this event. During this event, the Parker Solar Probe was 0.17 AU from the sun while ACE and STEREO-A were about 1 AU from the sun. This event originated from active region 12,738, which is about 80 degrees east of PSP nominal solar magnetic footprint (Malandraki et al. 2023).

Spacecraft	Distance From Sun [AU]	Start Carrington Longitude [°]	End Carrington Longitude [°]
PSP	0.17	354.2	358.4
ACE	1	98.6	63.8
STEREO-A	0.97	352.2	326.0

Table 3.1: Spacecraft distance from sun, and start an end Carrington Longitude

Figure 3.1 shows the positions of the spacecrafts in relation to each other, to the sun, and their nominal parker spiral connection during this event. At the beginning of this event, STEREO-A and the PSP were separated by 2°and by the end of the event STEREO-A and PSP were separated by 32.4°, within the expected amount of longitudinal spread for an impulsive SEP event if STEREO-A and PSP were centered over the active region. If the event did not occur in the middle of the

separation between PSP and STEREO-A, the spread of the event might miss one or both of the spacecrafts. Although STEREO-A and PSP have close Carrington longitudes, their nominal parker spirals are not necessarily in close proximity. It is reasonable to expect to see activity from this event at PSP and STEREO-A given their relative locations. PSP and ACE were separated by 95°at the beginning of the event and by 60°by the end of the event, so it would be less likely to see activity from this event at ACE. The active region that produced this flare was located at a Carrington longitude of 292°(Leske et al. 2019).Active region 12,738 is separated from PSP by 63.2°.

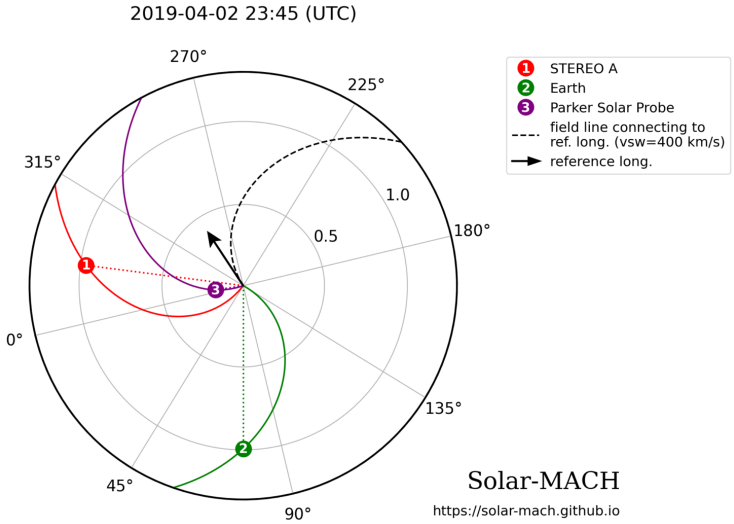

Figure 3.1: Positions of Spacecraft in relation to each other, the sun, and their nominal Parker spiral. ACE orbits L1, so the position of the Earth is used to represent the position of ACE. The black arrow represents the longitude of the flaring active region. Plot produced using Solar-MACH (Gieseler et al. 2022).

^{3}He/^{4}He Ratios

Figure 3.2 plots the ^{3}He/^{4}He ratio at PSP during the first event. The x-axis is the duration of the event plotted against the average energy of ^{4}He on the y-axis. The color bar indicates the ^{3}He/^{4}He ratio plotted on a log scale. The background solar wind ^{3}He/^{4}He ratio values are on the order of 10^{-4} (Reames 2021, Mewaldt et al. 2008). During impulsive events, the ^{3}He/^{4}He ratio can be enhanced as much as 1000x - 10,000x the background solar wind levels (Malandraki and Crosby 2018). The maximum ratio is on the order of 10^2, which meets and even exceeds the amount of enhancement expected for an impulsive event, indicating that the first event is impulsive.

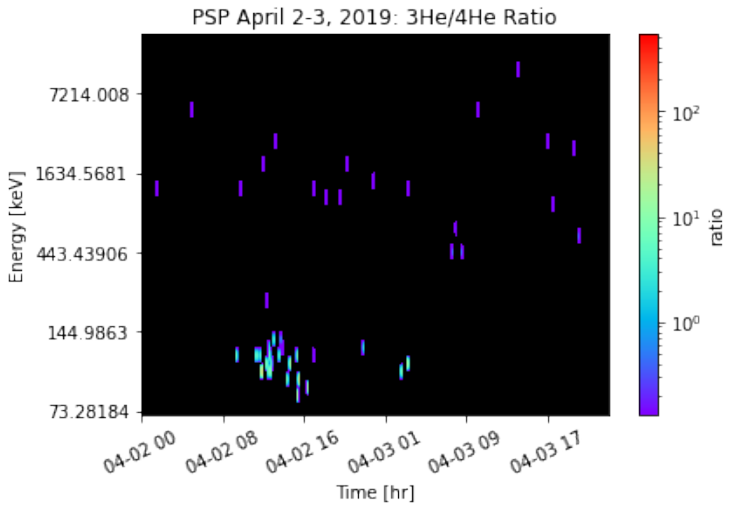

Figure 3.2: The ^{3}He/^{4}He Ratios measured by PSP during event 1. The ratio is relatively high indicating that this event can be classified as an Impulsive event.

Time-Intensity Profiles

Figures 3.3-3.7 are the time analysis plots for this event from PSP, ACE, and STEREO-A. Figures 3.3-3.6 are stacked time-analysis plots. The stacked plots contain two types of analysis, one is the time-intensity profiles (mentioned in Chapter 1). Time-intensity profiles plot the time over the event on the x-axis and the flux of the ion on the y-axis (log-scaled). In the following stacked plots in this chapter, He is plotted on one plot (if ^{3}He and ^{4}He are both available, they are plotted on the same plot), and Fe, C, and O are plotted on the same plot. The other type of plot is a color bar plot similar to the ^{3}He/^{4}He ratio plots, the x-axis is the time over the event, the y-axis is the average energy the ions were measured at, and the color bar indicates the flux on a log scale. This type of analysis indicates to what energies the ions are being accelerated and the beginning and end of the event. These plots are stacked on top of each other to make time-dependent structure more evident. The stacked plots contain 6 or 7 plots, two time-intensity profiles (He and the heavy ions) and color bar plots for He (^{3}He and ^{4}He when available), Fe, C, and O. This type of stacked plot makes time analysis of phenomena across multiple properties easy to see.

Figure 3.3 is the stacked time analysis plot for Event 1 measured at PSP. At Parker Solar Probe, ion fluxes increase around 12pm on April 2nd and begin to decrease to background levels around 6pm on April 3rd. This indicates that at PSP, Event 1 begins around 12 pm on April 2nd, and ends around 6pm April 3rd. In the time-

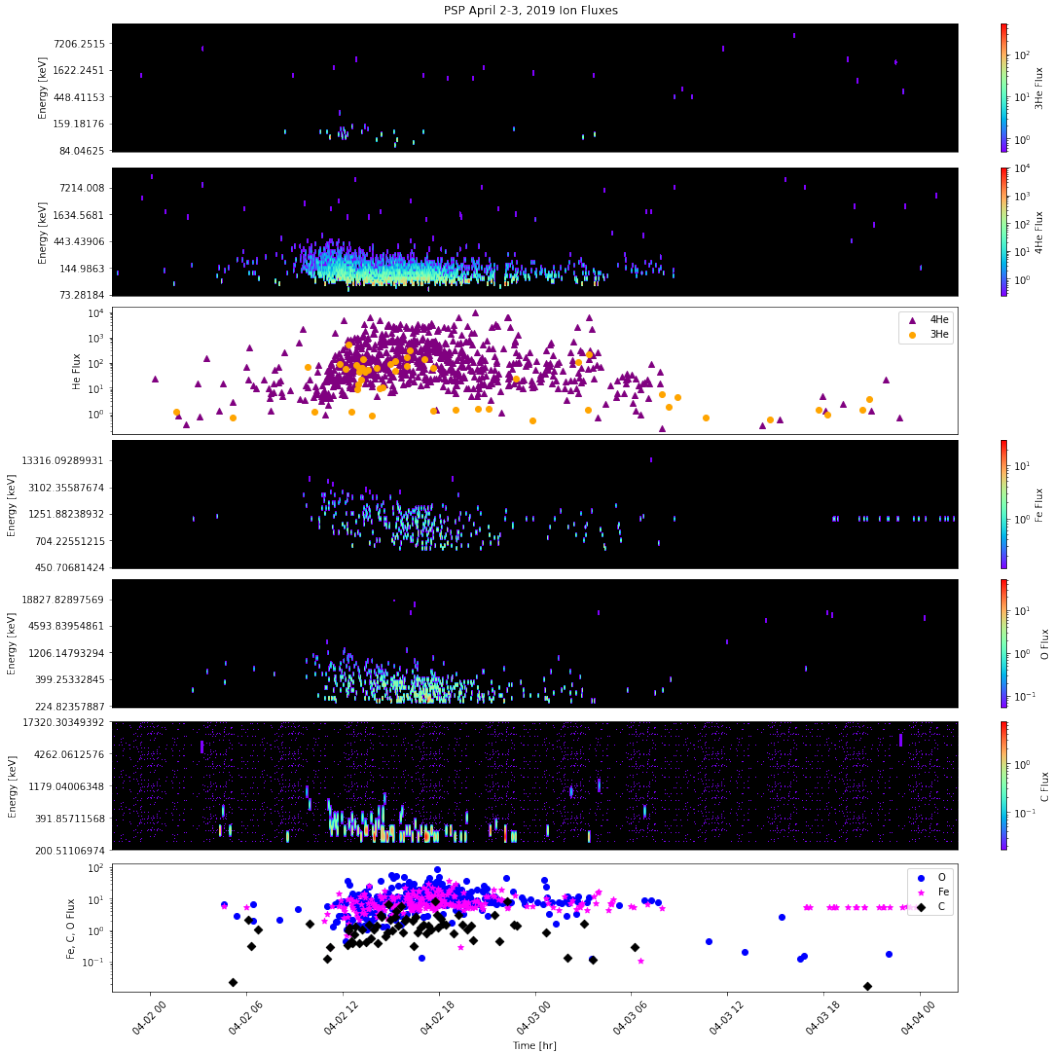

Figure 3.3: Event 1 (April 2-3, 2019) time analysis stacked plots at PSP.

intensity profiles, this event had a low enhancement of ^{3}He, but high enhancements in the heavy ions. This is mirrored in the color bar plots, where most of the ^{3}He flux measured falls into the very lower portion of the ^{3}He EPI-lo energy range, but EPI-Lo measured heavy ion flux over a greater portion of the ion's EPI-lo energy range. There is a strong presence of Fe flux compared to O, but ^{3}He flux is weaker compared to ^{4}He flux. Despite this, there is an evident time-dependent structure indicated by a sharp increase in flux on the time-intensity plots at the onset of the event. EPI-Lo has an energy range of 20 keV/nuc - 20 MeV/nuc, and many of the particles accelerated seem to remain in the lower part of the energy range at less than 10 MeV/nuc. It is clear, especially from the C and ^{4}he flux (panel 6 and panel 2) that ions are being accelerated to lower energies rather than higher energies (higher

flux concentrated at the bottom of the plot where there are lower energies).

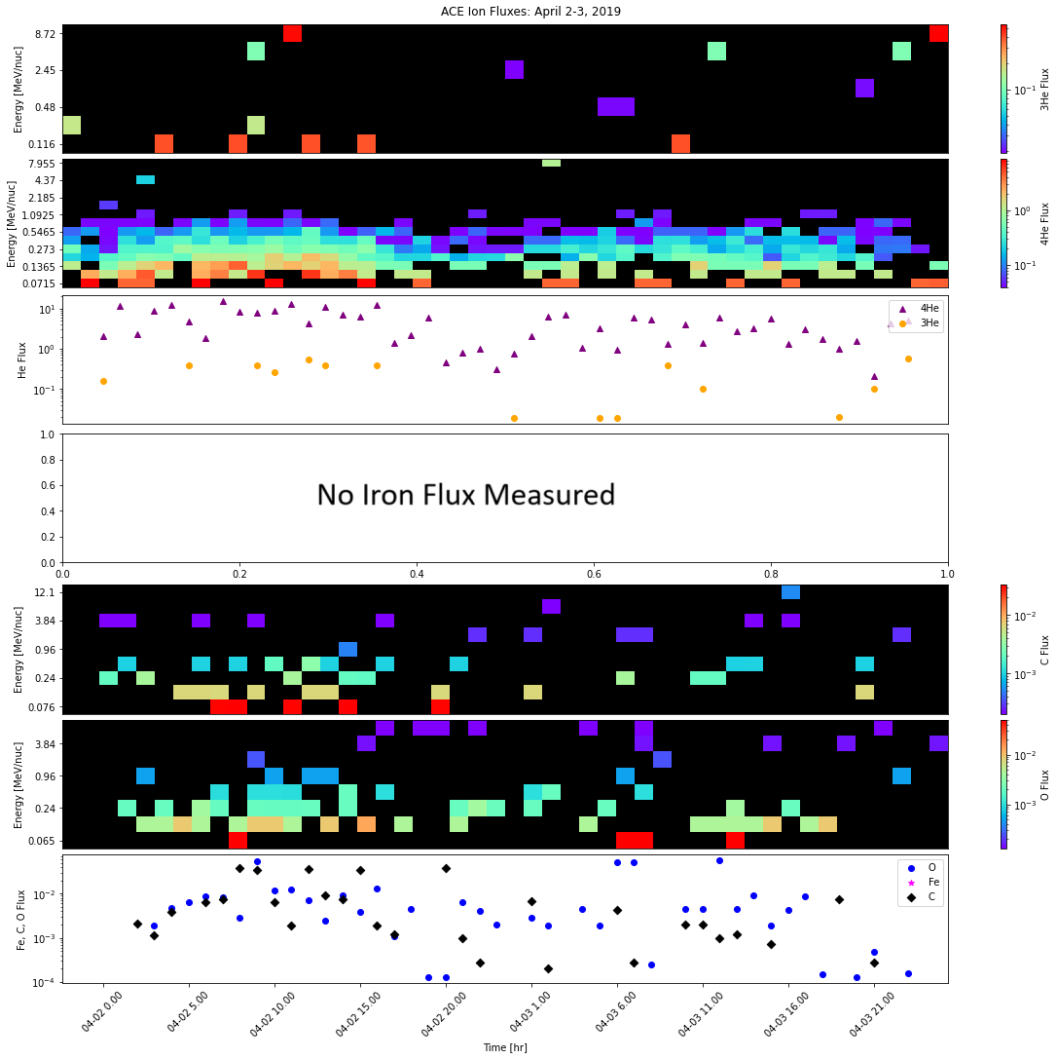

Figure 3.4: Event 1 (April 2-3, 2019) time analysis stacked plots at ACE.

Figure 3.4 is the stacked time analysis plot for Event 1 measured at ACE. ACE was located outside the expected longitudinal range of an impulsive event (95°at the beginning and 60°at the end). ACE has both a smaller energy resolution and time resolution, so the color bar plots look less detailed. At ACE, there is no clear time-dependent structure. Additionally, the fluxes measured are not that much higher than background fluxes if ACE were to have seen this event, there would have been a time delay after what was seen at PSP (i.e. the ion fluxes would have peaked later at ACE than at Parker Solar Probe because ACE is both longitudinal and radially farther away from the active region than PSP is). The empty panel is panel 4, where iron fluxes would be recorded. There is no iron flux measured, which may be because of

the lower energy resolution but is also an indication that ACE did not pick up this event.

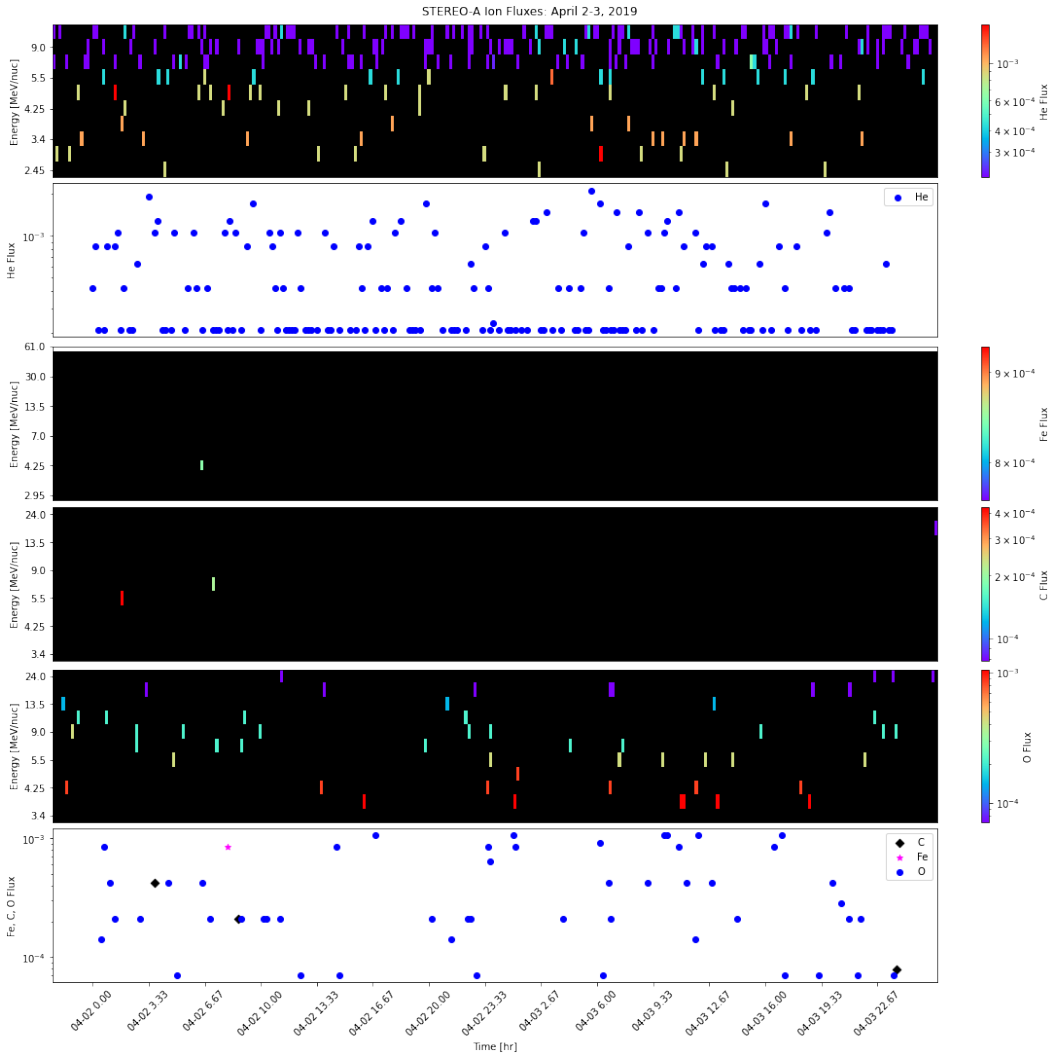

Figure 3.5: Event 1 (April 2-3, 2019) time analysis stacked plots at STEREO-A.

Figure 3.5 is the stacked time analysis plots for Event 1 measured at STEREO-A. Although PSP and STEREO-A were very close longitudinally, their nominal Parker spirals were not necessarily close enough to expect to see Event 1 at STEREO-A. Additionally, STEREO-A does not distinguish between ^{3}He and ^{4}He, so although there was significant intensity of He, it is not clear if there was increased intensity of ^{3}He. Additionally, the Helium intensity is not significantly higher than background levels (first panel). There are also no significant enhancements in any of the heavier ions (panel 3-5). This coupled with the fact that there is no time-dependent structure indicated that STEREO-A did not pick up this event.

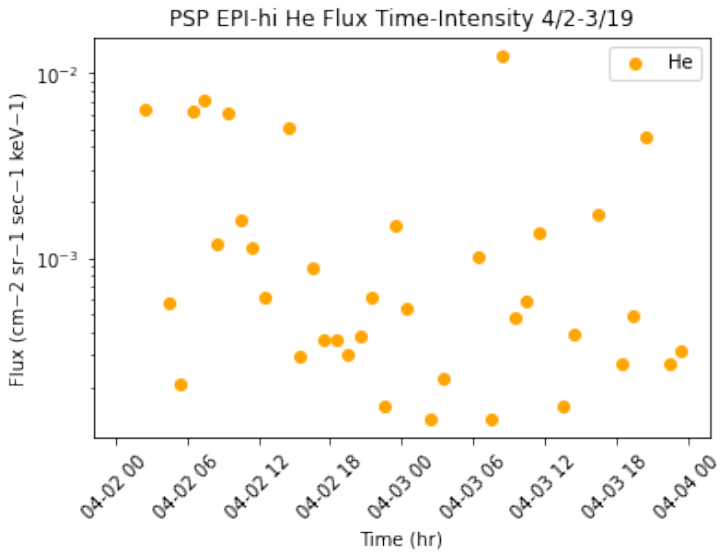

Figure 3.6: PSP EPI-Hi Time-Intensity Profile during the first event, summed over the entire energy range. Shows slight enhancements in He, but no discernible time-dependent structure.

Interestingly, although PSP and STEREO-A are longitudinally close, there is no significant activity at STEREO-A higher than background levels. This may be because STEREO-A was much farther away from the sun than the PSP was. This increased radial distance would allow for more cross-field diffusion to occur, essentially dropping the 'event-level' fluxes seen at PSP, to background levels at STEREO-A. However, STEREO-A LET also has a slightly higher energy range (1.8 MeV/nuc to 70 MeV/nuc) than PSP. Much of the elevated flux intensity measured at PSP was concentrated to the lower half of the EPI-Lo energy range which is at a keV magnitude rather than an MeV magnitude. This indicates a possible energy dependence with ions only being accelerated to low energies and thus not being seen by STEREO-A LET. This is further corroborated by measurements at EPI-Hi which has a comparable energy range (1 to 100 MeV/nuc) to STEREO-A LET. While EPI-Hi picked up elevated intensity of He (pictured in Figure 3.6), there was no discernible time-dependent structure. Whether an event occurred could not be determined just by using EPI-Hi data. Finally, Malandraki et al. (2023) also found that this event was only observed at lower energies.

3.2 Event 2: April 4, 2019

The second event occurred on April 4, 2019. It was also identified by the Parker Solar Probe in Mitchell et al. (2023). Below, in Table 3.2, are the distance from the sun, the start Carrington longitude, and the end Carrington longitude of each of the spacecraft during this event. During this event, the Parker Solar Probe was 0.17 AU from the sun while ACE and STEREO-A were about 1 AU from the sun. This event also originated from active region 12,738, which has a Carrington longitude of 292°(Leske et al. 2019).

Spacecraft	Distance From Sun [AU]	Start Carrington Longitude [°]	End Carrington Longitude [°]
PSP	0.17	358.4	3.0
ACE	1	63.2	50.2
STEREO-A	0.97	325.9	312.9.0

Table 3.2: Spacecraft distance from sun, and beginning and end Carrington Longitude.

Figure 3.7 shows the positions of the spacecraft in relation to each other and to the sun and their nominal Parker spiral during this event. At the beginning of the second event, STEREO-A and the PSP were separated by 32.5°and by the end of the event STEREO-A and the PSP were separated by 49.6°, within the expected amount of longitudinal spread for an impulsive SEP event. Additionally, PSP and STEREO-A's nominal parker spirals are close together, but increasing when compared to event 1. Depending on energy dependences, total amount of spread at initiation of the event, and other transport-dependent factors we might expect see activity from this event at PSP and STEREO-A just due to the proximity of their nominal Parker spirals. PSP and ACE were separated by 64.8°at the beginning of the event and by 47.7°by the end of the event, so again, it would be less likely/ more surprising to see this event at ACE. Active region 12,738 is separated from PSP by about 60°.

^{3}He/^{4}He Ratios

Figure 3.8 plots the ^{3}He/^{4}He ratio at PSP during the second event. The x-axis is the duration of the event plotted against the average energy of ^{4}He on the y-axis. The color bar indicates the ^{3}He/^{4}He ratio plotted on a log scale. The background solar wind ^{3}He/^{4}He ratio values are on the order of 10^{-4} (Reames 2021, Mewaldt et al. 2008). The maximum ratio is on the order of 10^0, which just meets the amount of enhancement expected for an impulsive event, indicating that the first event is

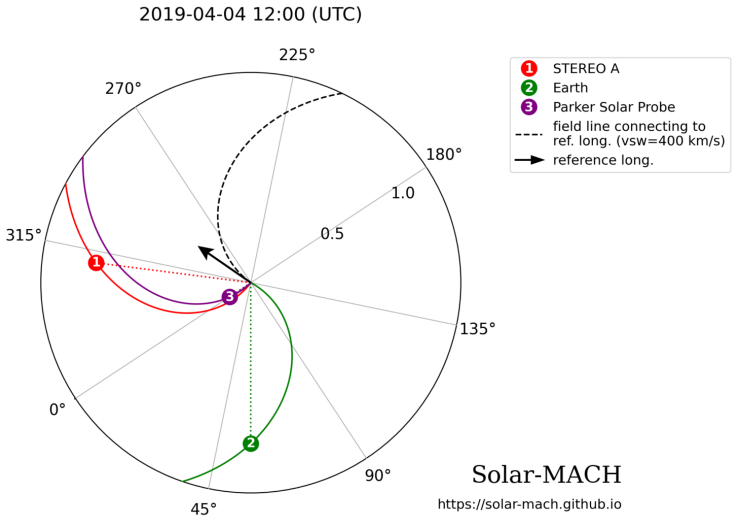

Figure 3.7: Positions of Spacecraft in relation to each other, the sun, and their nominal Parker spiral in the middle of Event 2. ACE orbits L1, so the position of the Earth is used to represent the position of ACE. The black arrow represents the longitude of the flaring active region. Plot produced using Solar-MACH (Gieseler et al. 2022).

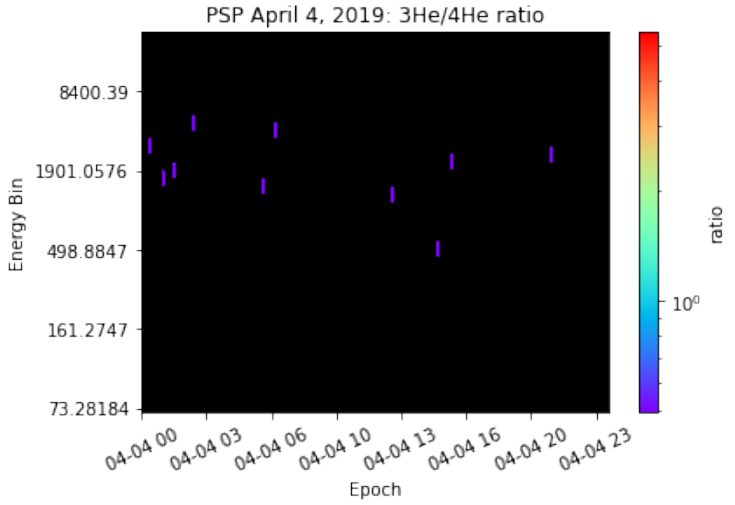

Figure 3.8: The ^{3}He/^{4}He Ratios measured by PSP during event 2. The ratio is slightly lower than expected for an impulsive event.

impulsive. This event had very low enhancements of ^{3}He, so the ^{3}He/^{4}He ratio is lower than expected for an impulsive event.

Time- Intensity Profile

Figures 3.9-3.12 are the time analysis plots for this event from PSP, ACE, and STEREO-A. Figures 3.9, 3.11, and 3.12 are stacked time-analysis plots. And Figure 3.10 is the PSP EPI-Hi Helium time-intensity profile for this event. These figures follow the same structure as the Figures in the Event 1 section.

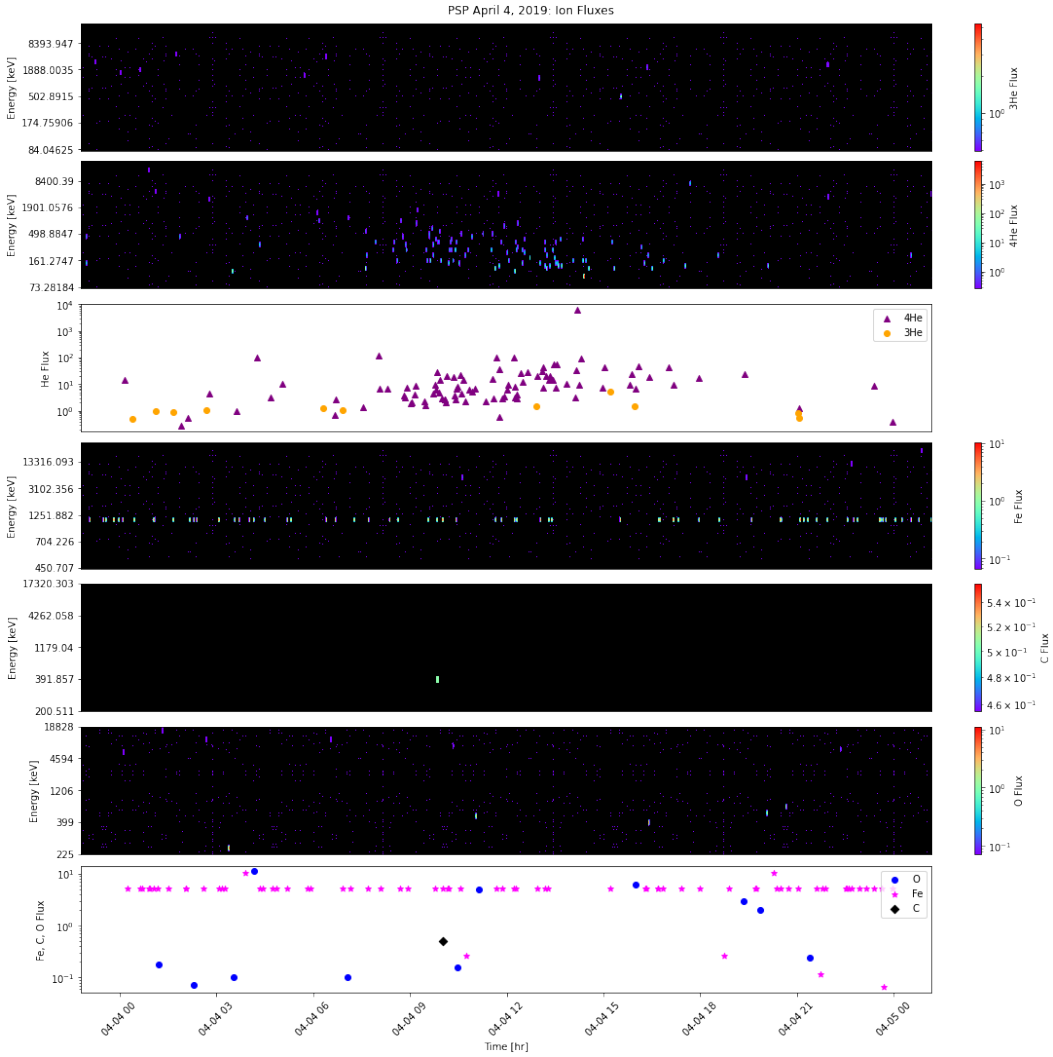

Figure 3.9: Event 2 (April 4, 2019) time analysis plots at PSP.

Figure 3.9 is the stacked time analysis plot for Event 2 measured at PSP. At Parker Solar Probe, ^{4}He fluxes increase around 9 am on April 4th and begin to decrease to background levels around 6pm on April 4th. This indicates that in the EPI-Lo energy range (20 keV - 20 MeV), begins around 9 am on April 4th and end around 6pm on April 4th. Time-dependent structure only appears in ^{4}He (second panel). Although there is a measurable amount of ^{3}He in this event, it is near background

levels, and enhancements are low when compared with ^{4}He. Additionally, this event did not produce any heavier ions (panel 4-6) above background levels. The presence of low flux ^{3}He and no significant heavy ions, while in consideration of the same active region led to the classification of an impulsive SEP, but it is an extremely weak event.

Interestingly, this event also appears to have an energy dependence in the opposite direction as the first event. Although this event has a minimal time-dependent structure in the EPI-Lo energies, EPI-Hi shows a strong time-dependent structure. In the EPI-Hi energy range, the event appears to begin about six hours earlier, around 3 am April 4th. Figure 3.10 shows the time-intensity profile for He summed over the EPI-Hi energy range.

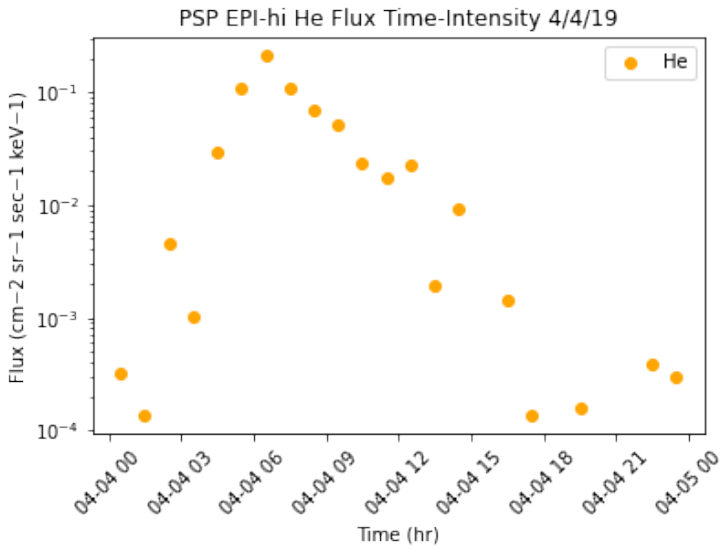

Figure 3.10: PSP EPI-Hi Time-Intensity Profile during the second event, summed over the entire energy range. Shows strong time-dependent structure in He, but low fluxes.

Although there is a more evident time-dependent structure in the EPI-Hi energy range, the summed flux values are an order of magnitude lower than the summed flux values in the EPI-Lo energy range, so less ions are being accelerated to higher energies. PSP was only 0.17 AU from the sun during this event. These observations, when understood in conjunction with Event 1 (they originate from the same active region) indicate this was most likely a very weak flare, but the acceleration mechanism was seeded by the low energy ions from the first, essentially re-accelerated what was accelerated the first time in Event 1.

ACE was at a Carrington longitude outside the expected longitudinal spread for an impulsive SEP event. Figure 3.11 shows the time-analysis plots at ACE. Although there appears to be some time-dependent structure, particularly in ^{4}He (panel 2), it is unlikely that ACE picked up the event seen by PSP. This is not unexpected for a weak event near the sun. Once the particles expanded volumetrically and diffused longitudinally and latitudinally into space, it would be hard to identify any corresponding time variation at 1 AU.

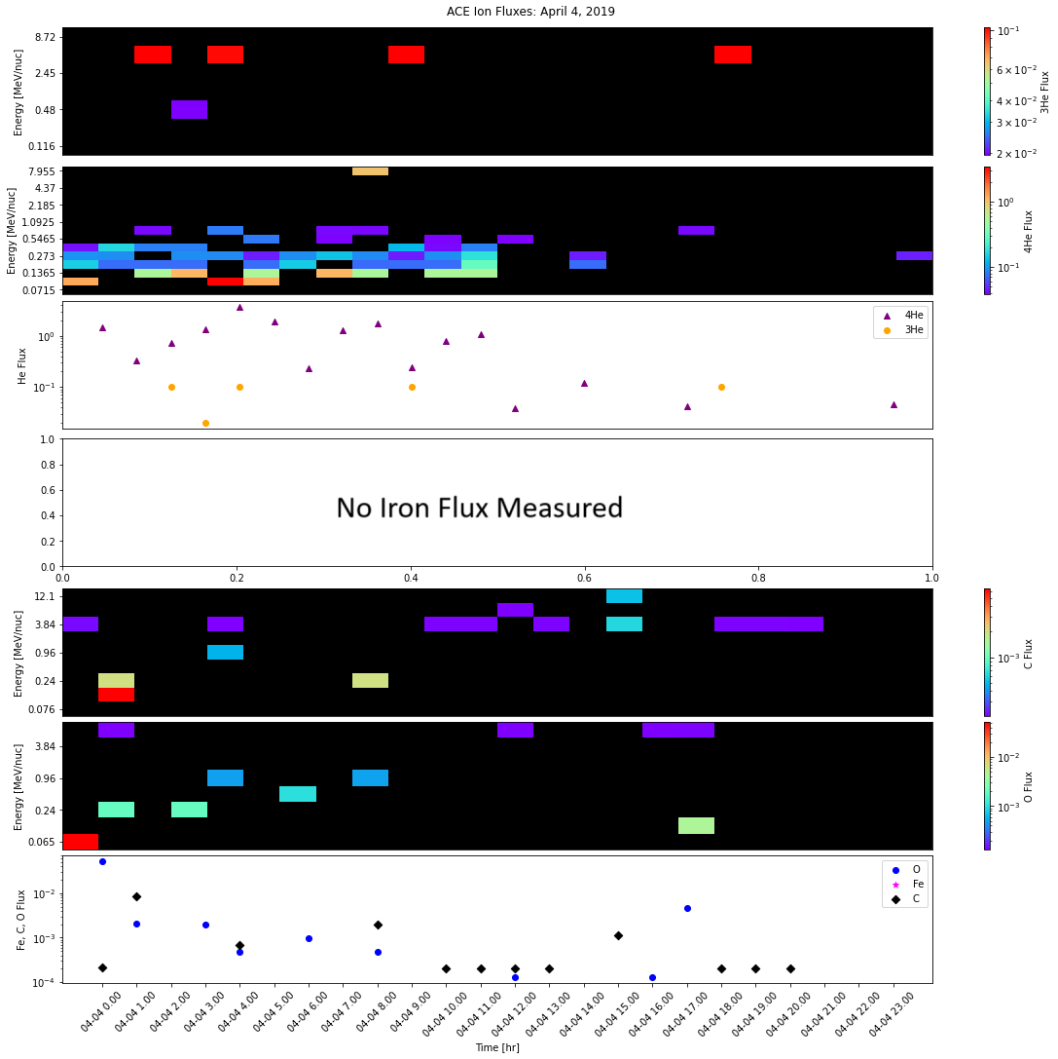

Figure 3.11: Event 2 (April 4, 2019) time analysis plots at ACE.

STEREO-A's nominal parker spiral is very close to PSP's nominal parker spiral. Due to this, we might expect to see activity from the second event at STEREO-A as well. Figure 3.12 shows time analysis plots at STEREO-A for this event. However, there are just slightly elevated counts. Remember that EPI-Hi's energy range is more

comparable to STEREO-A LET. However, despite seeing a strong time-dependent structure in EPI-Hi (Figure 3.10), there is no discernible structure in STEREO-A. This is not necessarily surprising given the flux levels at EPI-Hi were very low and STEREO-A is located 0.8 AU away from PSP. As the particles from the second event continue to propagate out, their flux becomes lower as they diffuse through the interplanetary medium. All this indicates STEREO-A also did not pick up this event.

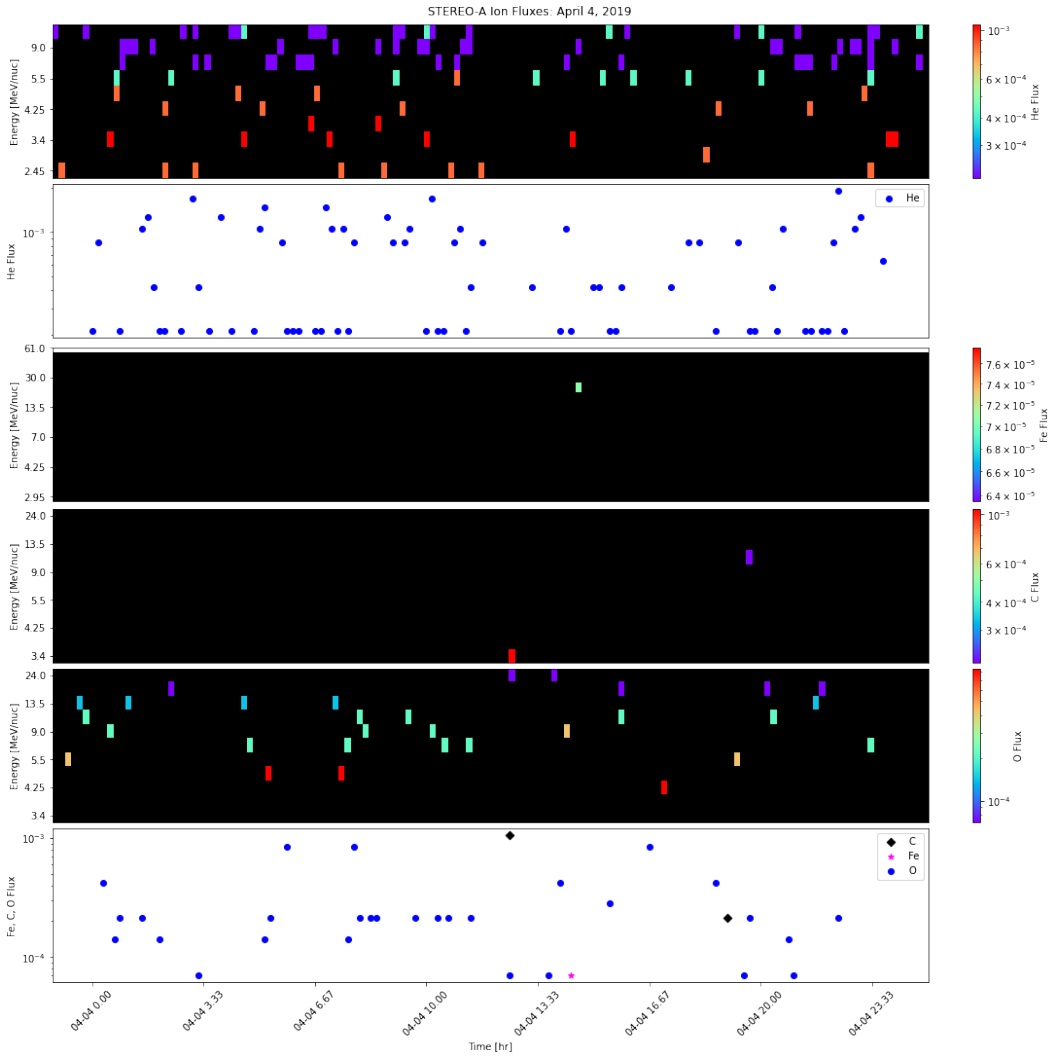

Figure 3.12: Event 2 (April 4, 2019) time analysis plots at STEREO-A.

3.3 Event 3: April 20-23, 2019

The third event occurred from April 20-23, 2019. It was also identified by the Parker Solar Probe in Mitchell et al. (2023). Below, in Table 3.3, are the distance from the sun, the start Carrington longitude, and the end Carrington longitude of each of the spacecraft during this event. During this event, the Parker Solar Probe was 0.45 AU from the sun while ACE and STEREO-A were about 1 AU from the sun. It is not clear where this event originated from, although given its proximity to Event 1 and Event 2 it may have originated from the same active region.

Spacecraft	Distance From Sun [AU]	Start Carrington Longitude [°]	End Carrington Longitude [°]
PSP	0.45	271.6	223.8
ACE	1	212.0	159.3
STEREO-A	0.97	115.4	62.9

Table 3.3: Spacecraft distance from sun, and beginning and end Carrington Longitude.

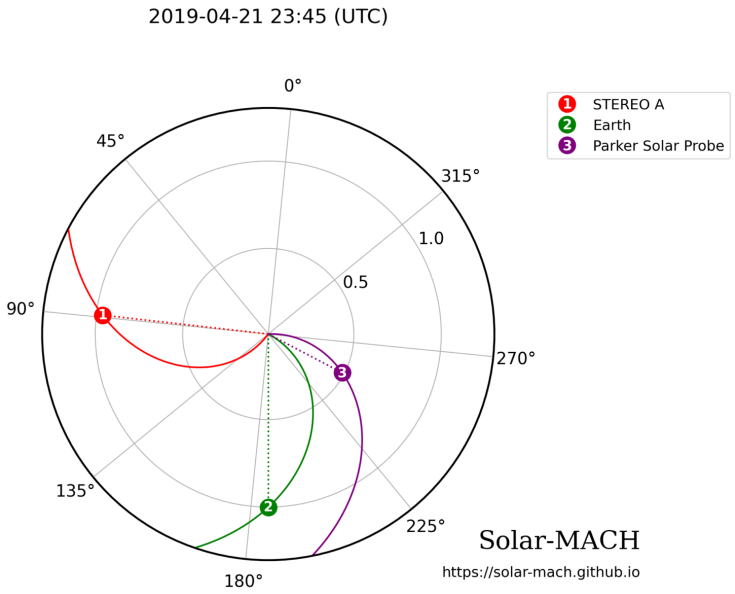

Figure 3.13: Positions of Spacecraft in relation to each other, the sun, and their nominal Parker spiral in the middle of Event 3. ACE orbits L1, so the position of the Earth is used to represent the position of ACE. Plot produced using Solar-MACH (Gieseler et al. 2022).

Figure 3.13 shows the positions of the spacecrafts in relation to each other and to the sun and their nominal parker spiral during this event. At the beginning of this event, STEREO-A and the PSP were separated by 156.23°and by the end of the

event STEREO-A and the PSP were separated by 160.89°, outside the expected amount of longitudinal spread for an impulsive SEP event. It would be less likely/ more surprising to see this event at STEREO-A. The PSP and ACE were separated by 59.61°at the beginning of the event and by 64.5°degrees by the end of the event. Additionally, PSP and ACE's nominal parker spirals are very close together. It would not be surprising to see activity from this event at PSP and ACE due to the proximity of their nominal parker spirals.

^{3}He/^{4}He Ratios

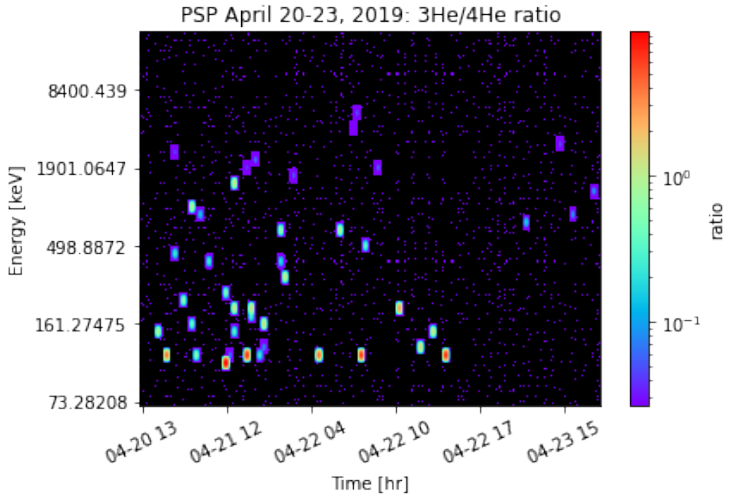

Figure 3.14: The ^{3}He/^{4}He Ratios measured by PSP during event 3. The ratio is expected for an impulsive event.

Figure 3.14 plots the ^{3}He/^{4}He ratio at PSP during the third event. The x-axis is the duration of the event plotted against the average energy of ^{4}He on the y-axis. The color bar indicates the ^{3}He/^{4}He ratio plotted on a log scale. The background solar wind ^{3}He/^{4}He ratio values are on the order of 10^{-4} (Reames 2021, Mewaldt et al. 2008). The maximum ratio is on the order of 10^0-10^1, which meets the amount of enhancement expected for an impulsive event, indicating that this event is impulsive.

Time- Intensity Profile

Figures 3.15-3.18 are the time analysis plots for this event from PSP, ACE, and STEREO-A. Figures 3.15, 3.17, and 3.18 are stacked time-analysis plots. Figure 3.16 is the PSP EPI-Hi Helium time-intensity profile for this event. These figures follow the same structure as the Figures in the Event 1 and Event 2 sections.

Figure 3.15 is the stacked time analysis plot for Event 3 measured at PSP. The third

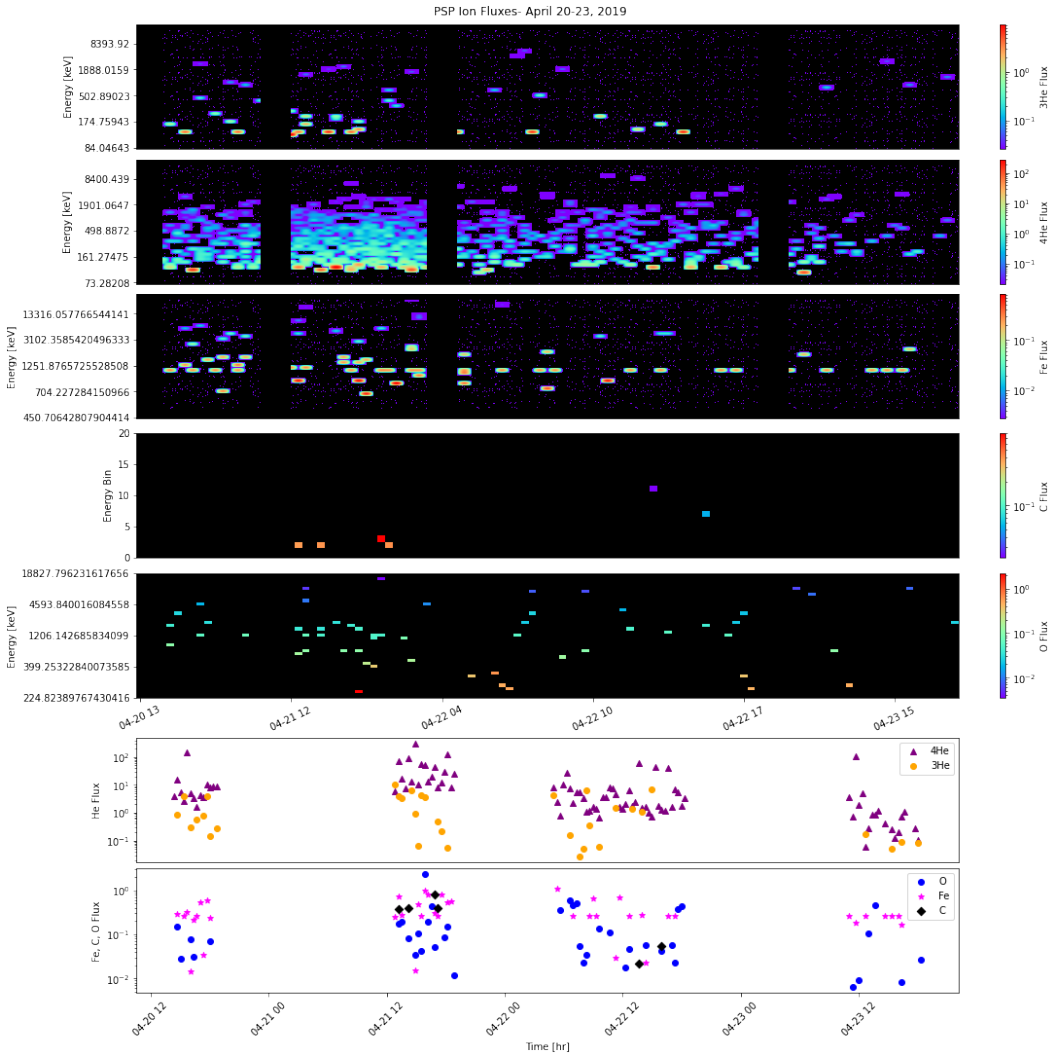

Figure 3.15: Event 3 (April 20-23, 2019) time analysis plots at PSP.

event was also identified by the Parker Solar Probe. The time resolution for PSP in this event was much lower than the other PSP time resolutions. During the three-day period of this event, measurements were taken on average every 39 minutes giving Event 3 a lower time resolution than the other events measured at PSP. A reason for this may be because PSP periodically turns off its instruments to send data back to Earth and perform other mission-critical tasks that require power off. This event appears to peak in the EPI-Lo energy range around 1 pm on April 21, 2019. 3He fluxes reach an order of magnitude of 10^1, and Fe fluxes reach an order of magnitude of about 10^0. There is some time-dependent structure seen in the EPI-Lo energy range. Elevated intensity of ^{3}He and the heavy ions persist over the duration of the event.

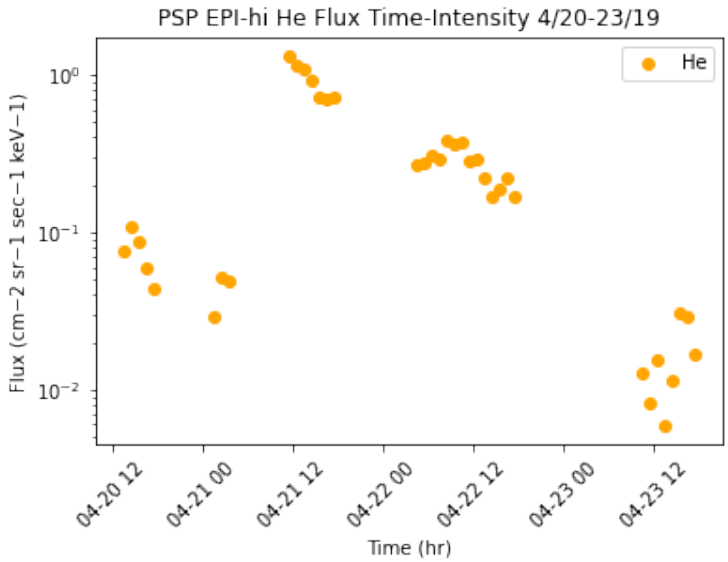

Figure 3.16: PSP EPI-Hi Time-Intensity Profile during the third event, summed over the entire energy range. Shows strong time-dependent structure in He.

There is a dramatic time-dependent structure observed in the Helium EPI-Hi time-intensity plot (pictured in Figure 3.16), including a sharp peak in He intensity at the onset of the event which appears to be an hour and a half earlier than the peak in the EPI-Lo energy range. Although there is a more clear time-dependent structure in the EPI-Hi time-intensity profile, the summed flux observed by EPI-Hi is two orders of magnitude lower than the summed fluxes observed by EPI-Lo. It is possible that PSP missed some initial flux at the beginning of this event as measurements begin April 20, 2019 at 12 pm rather than at 12 am. The varying onset times in EPI-Hi compared to EPI-Lo could indicate the distance to the source region, with high and low energy particles being created simultaneously but then due to their varying velocities arriving at PSP at different times, a multi-step acceleration mechanism, or some combination of the two. Further work would be required to distinguish between the cause of this time dependence.

In the beginning of this event, ACE was about 60°away from PSP, and at the end of this event, ACE was almost 65°away from PSP. Figure 3.17 shows the time-analysis plots for ACE. There is no clear time-dependent structure, but ACE measured elevated intensities of ^{3}He and the heavy ions. ACE's time resolution is a little better than PSPs in this event, and enhancements at ACE appear to begin earlier than at PSP, which could indicate this event reached ACE before PSP. There appears to be slightly elevated fluxes in ^{4}He and Fe around April 22, 2019. If this event

did reach ACE before PSP, this is a strong indicator of where this event may have originated from. Because of the elevated intensity of ^{3}He and Fe measured at ACE, it is very likely that ACE also picked up this event.

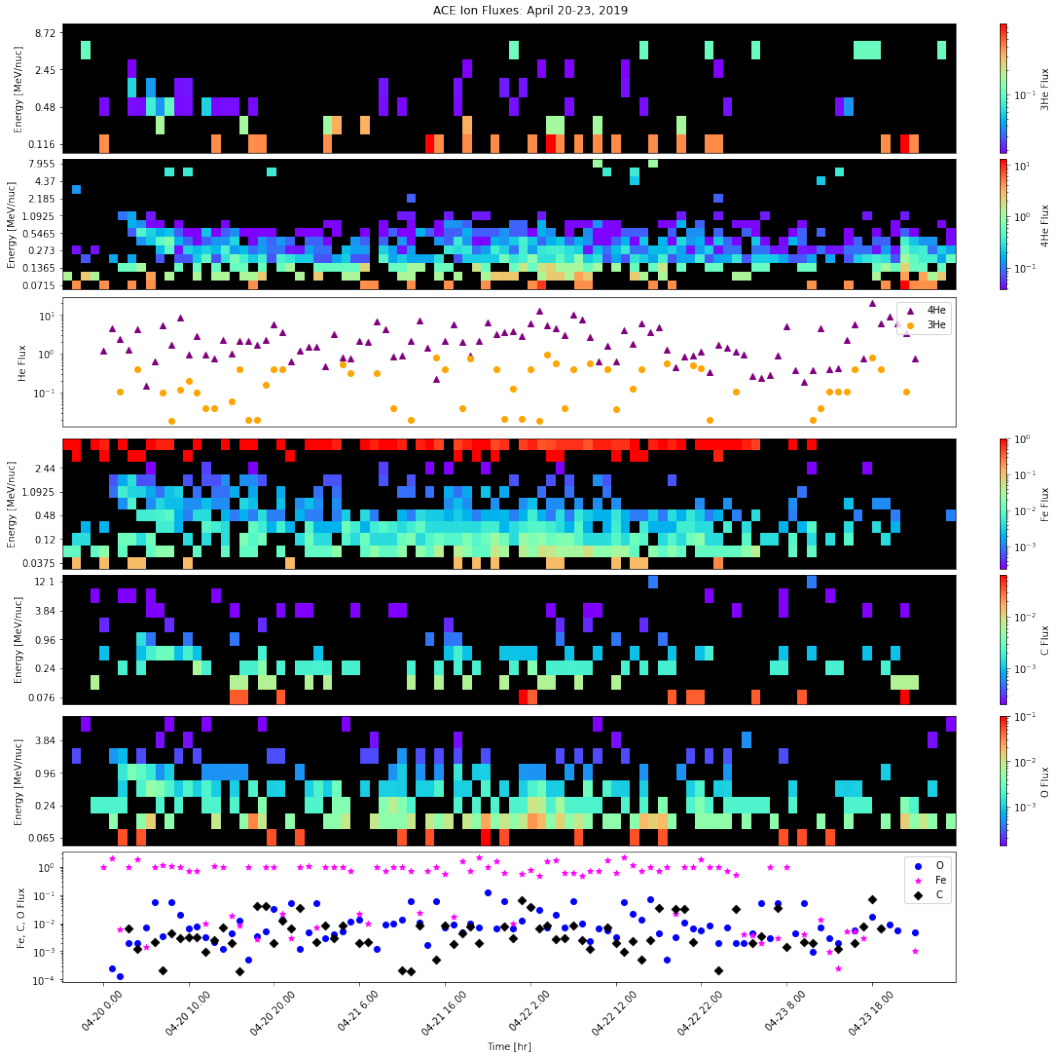

Figure 3.17: Event 3 (April 20-23, 2019) time analysis plots at ACE.

At the beginning of this event, STEREO-A was located 156°away from PSP. By the end of the event, STEREO-A was located 160 degrees away from PSP. Figure 3.18 is the time series analysis plots at STEREO-A from this event. At STEREO-A, this event showed no time-dependent structure or intensity above background levels of Helium or the heavy ions. There was no intensity of iron picked up at all. This indicates that STEREO-A did not pick up this event at all, which is to be expected as it was situated far outside the expected longitudinal range of an impulsive event.

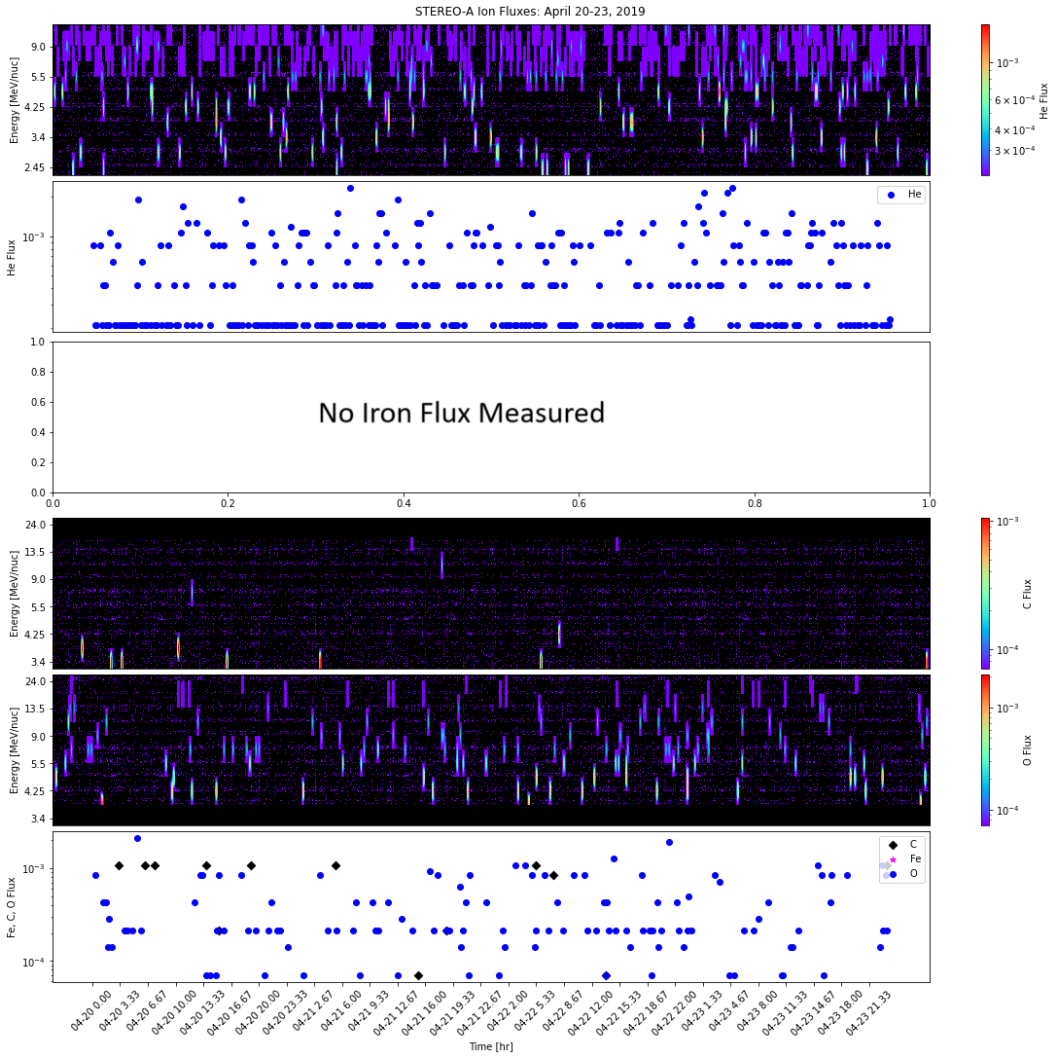

Figure 3.18: Event 3 (April 20-23, 2019) time analysis plots at STEREO-A.

3.4 Event 4: July 11, 2020

The fourth event occurred on July 11, 2020. It was identified by the Parker Solar Probe in Mitchell et al., (2023) and by Solar Orbiter in Mason et al., (2021). Table 3.4 lists the spacecraft distance from the sun, the start Carrington longitude, and the end Carrington longitude of each of the spacecraft during this event. During this event, the Parker Solar Probe was 0.73 AU from the sun, ACE and STEREO-A were about 1 AU from the sun, and SolO was the closest to the sun at 0.63 AU.

The two studies this event was identified in identify the duration of the event differ-

ently. Mason et al. (2021) identifies this event on July 11, 2020 with low intensities. Mitchell et al. (2023) identifies this event as spanning two days, from July 9, 2020 to July 11, 2020. This may indicate an event located near SolO and then diffusing to PSP, or that PSP and SolO saw two different events. There are further modeling efforts that could be done with existing tools to identify if it was a single event or two (or more), but that is outside the scope of this work.

Spacecraft	Distance From Sun [AU]	Start Carrington Longitude [°]	End Carrington Longitude [°]
PSP	0.73	80.2	66.9
ACE	1.02	56.5	43.4
STEREO-A	0.96	348.5	335.5
SolO	0.61	163.7	151.8

Table 3.4: Spacecraft distance from sun, and beginning and end Carrington Longitude.

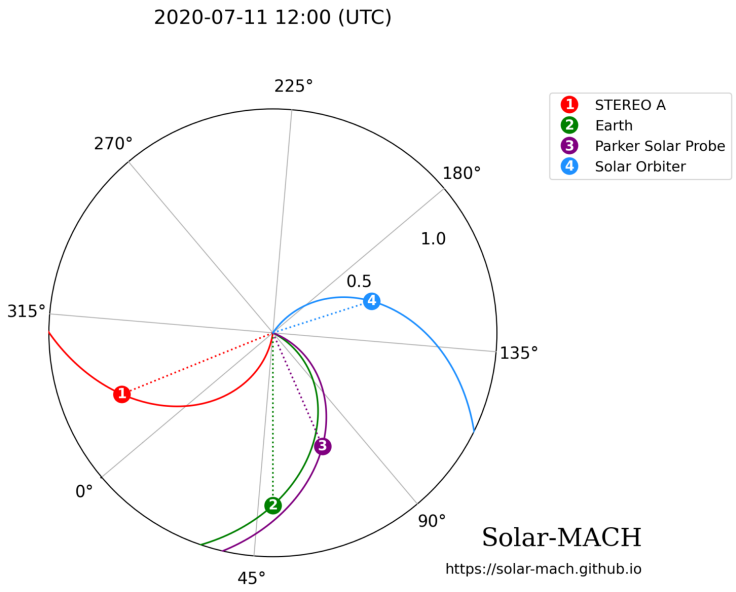

Figure 3.19: Positions of Spacecraft in relation to each other, the sun, and their nominal Parker spiral in the middle of Event 4. ACE orbits L1, so the position of the Earth is used to represent the position of ACE. Plot produced using Solar-MACH (Gieseler et al. 2022).

Figure 3.19 shows the positions of the spacecraft in relation to each other and to the sun and their nominal parker spiral during this event. At the beginning of this event, STEREO-A and the SolO were separated by 175.2°and by the end of the event STEREO-A and the SolO were separated by 176.8°, far outside the expected

amount of longitudinal spread for an impulsive SEP event. It would be less likely/ more surprising to see this event at STEREO-A. The SolO and ACE were separated by 107°at the beginning of the event and by 108.4°by the end of the event. PSP and SolO were separated by 83.7°at the beginning of the event and 84.9°by the end of the event. PSP and STEREO-A were separated by 92.2°at the beginning of the event and by 91.4°by the end of the event. PSP and ACE's nominal parker spirals were in close proximity during this event, and at the beginning of the event ACE and PSP were separated by 23.7°and 23.5°by the end of the event.

^{3}He/^{4}He Ratios

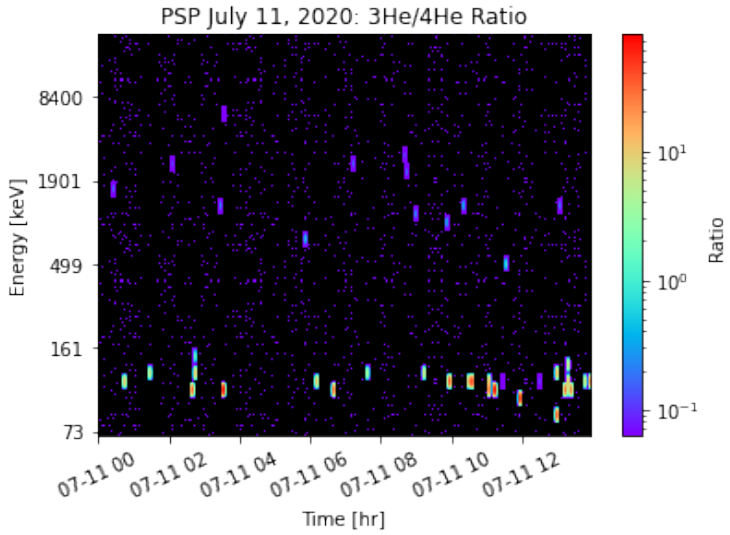

Figure 3.20: The ^{3}He/^{4}He Ratios measured by PSP during event 4. The ratio is expected for an impulsive event.

Figure 3.20 plots the ^{3}He/^{4}He ratio at PSP during the fourth event. The x-axis is the duration of the event plotted against the average energy of ^{4}He on the y-axis. The color bar indicates the ^{3}He/^{4}He ratio plotted on a log scale. The background solar wind ^{3}He/^{4}He ratio values are on the order of 10^{-4} (Reames 2021, Mewaldt et al. 2008). The maximum ratio is on the order of 10^1, which meets the amount of enhancement expected for an impulsive event, indicating that this event is impulsive. Mason et al. (2021) identifies this event as impulsive. Although Mason et al. (2021) and Mitchell et al. (2023) put the duration of the event at different lengths, measurements at PSP and SolO agree that this/these event(s) are impulsive.

Time-Intensity Profiles

Figures 3.21-3.25 are the time analysis plots for this event from PSP, ACE, and STEREO-A. Figures 3.21, 3.22, 3.24 and 3.25 are stacked time-analysis plots. Figure 3.23 is the PSP EPI-Hi Helium time-intensity profile for this event. These figures follow the same structure as the Figures in the other event sections.

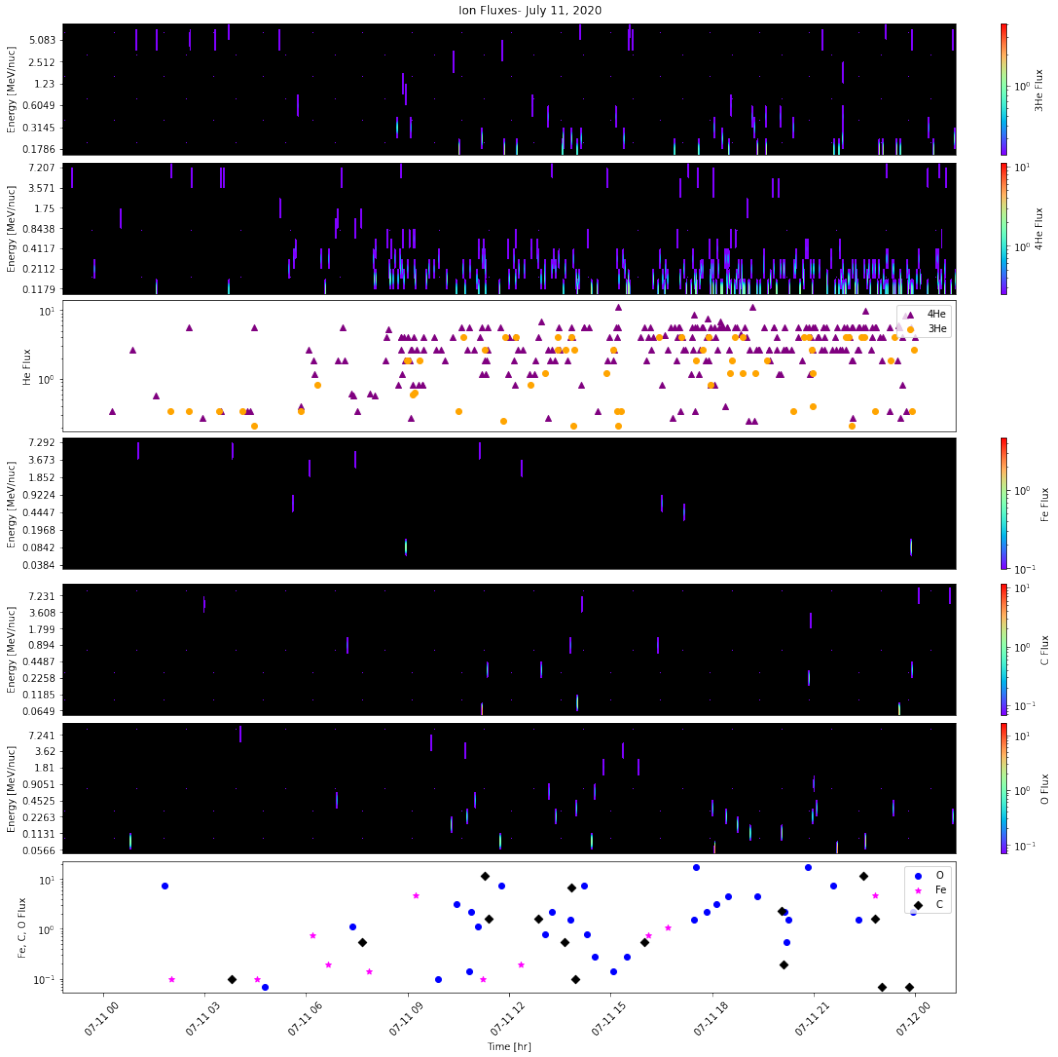

Figure 3.21: Event 4 (July 11, 2020) time analysis plots at SolO.

Figure 3.21 is the time series analysis plots at SolO for this event. The flux intensity during this event are elevated and peak around 10^1 cm^{-2} sr^{-1} sec^{-1} (keV/nuc)$^{-1}$ there is also some time-dependent structure. There is a gradual increase in ^{3}He, ^{4}He, and the heavy ions intensity beginning around 6 am on July 11, 2020. The maximum flux intensity measured at SolO during this event was 10 cm^{-2} sr^{-1} sec^{-1} (keV/nuc)$^{-1}$. Like Event 1 at PSP, ^{4}He and ^{3}He ions measured by SolO seem to

remain in the lower part of the SIS energy range, although there does not seem to be this same bias in the heavy ions.

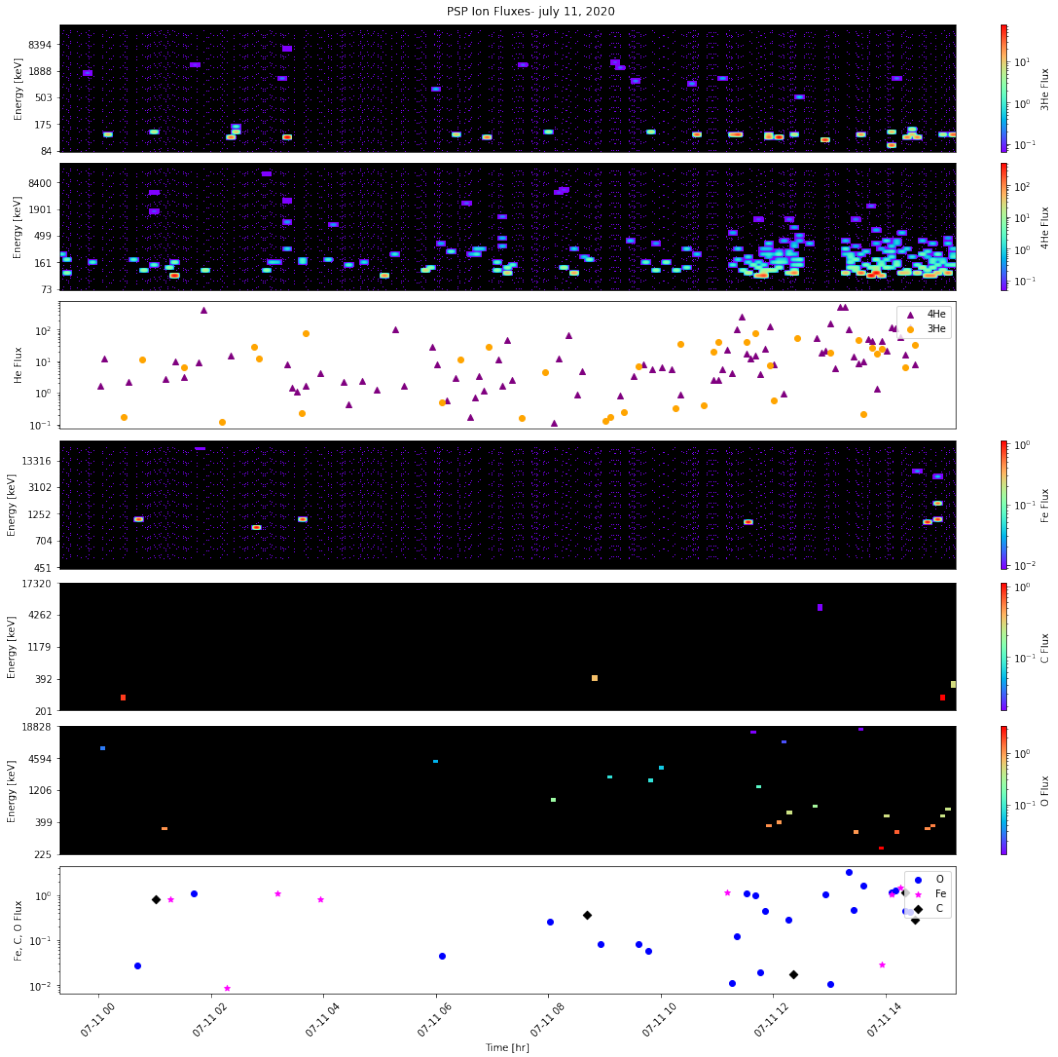

Figure 3.22: Event 4 (July 11, 2020) time analysis plots at PSP.

PSP also identified an event during this time period. Figure 3.22 is the time-series analysis plots at PSP for this event. The event measured at PSP does not show obvious time-dependent structure, although flux intensities at ^{3}He, ^{4}He, and O increase around 12 pm on July 11, 2020, six hours after the increase seen at SolO. Like at SolO, ^{4}He and ^{3}He ions measured by SolO seem to remain in the lower part of the EPI-Lo energy range. The maximum flux measured at PSP was in ^{4}He, at 10^{2} cm^{-2} sr^{-1} sec^{-1} (keV/nuc)$^{-1}$. Additionally, the heavy ions flux peaks around 10^{0} cm^{-2} sr^{-1} sec^{-1} (keV/nuc)$^{-1}$, around an order of magnitude lower than measured at SolO (Figure 3.21).

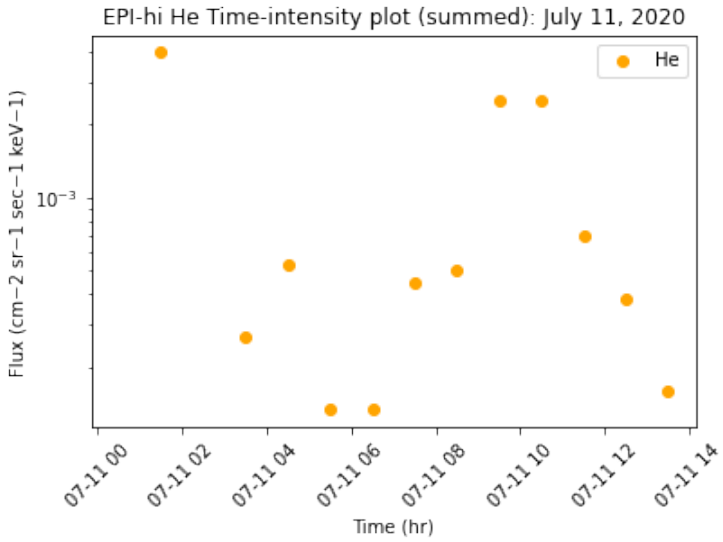

Figure 3.23: PSP EPI-Hi Time-Intensity Profile during the fourth event, summed over the entire energy range. Shows time-dependent structure in He.

There is a much more dramatic increase in He flux in the EPI-Hi energy range (Figure 3.23) during this event beginning around 7 am on July 11, 2020. Although there is a more evident time-dependent structure during this event, the summed flux intensities in the EPI-lo energy range are still a few orders of magnitude higher than the summed flux intensities in the EPI-Hi energy range.

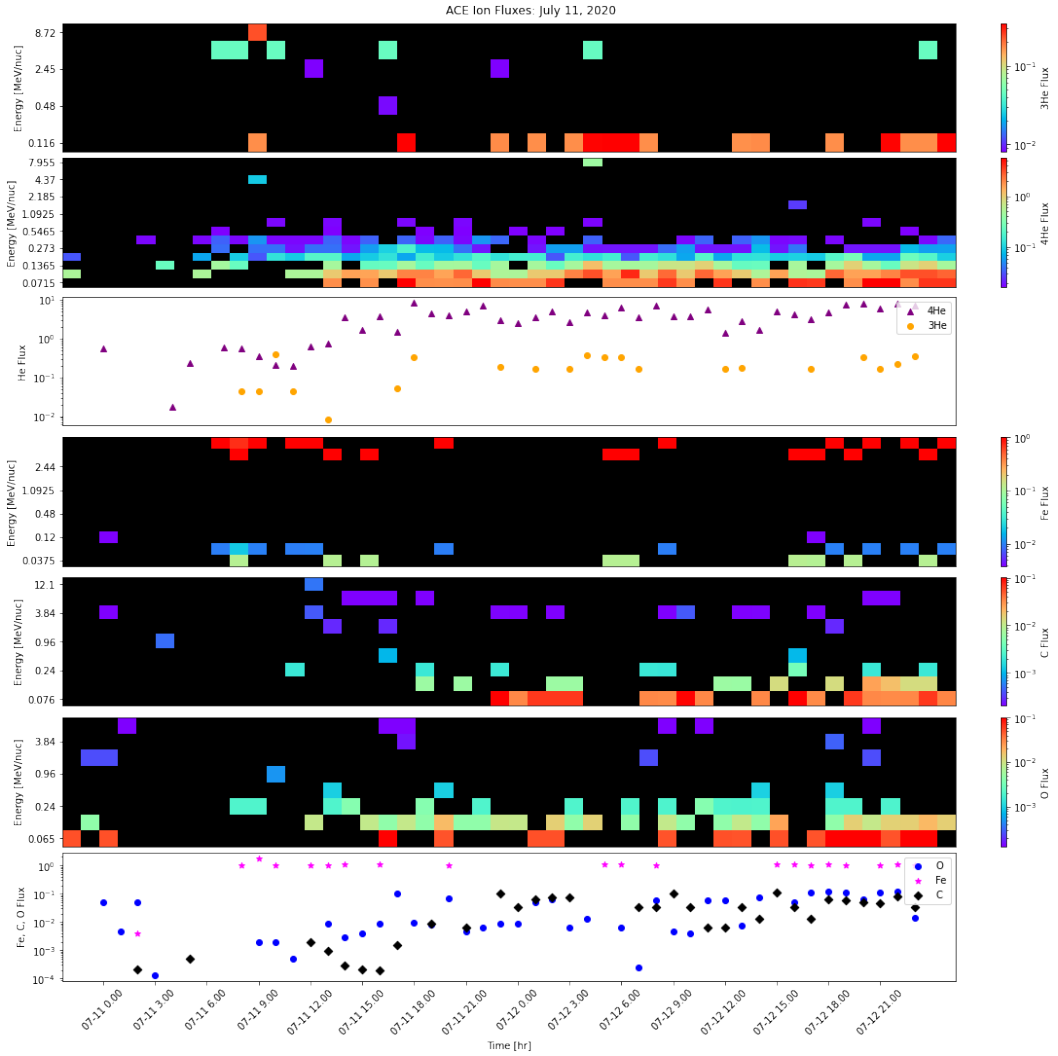

Figure 3.24: Event 4 (July 11, 2020) time analysis plots at ACE.

During this event, ACE was located on a nominal parker spiral very close to PSP's nominal parker spiral. Figure 3.24 is time- analysis data taken at ACE. Despite being radially farther away from the sun than PSP, ACE also sees slightly elevated flux intensities across all ions measured as well as some time time-dependent structure. The event seen by PSP at may also have been seen by ACE.

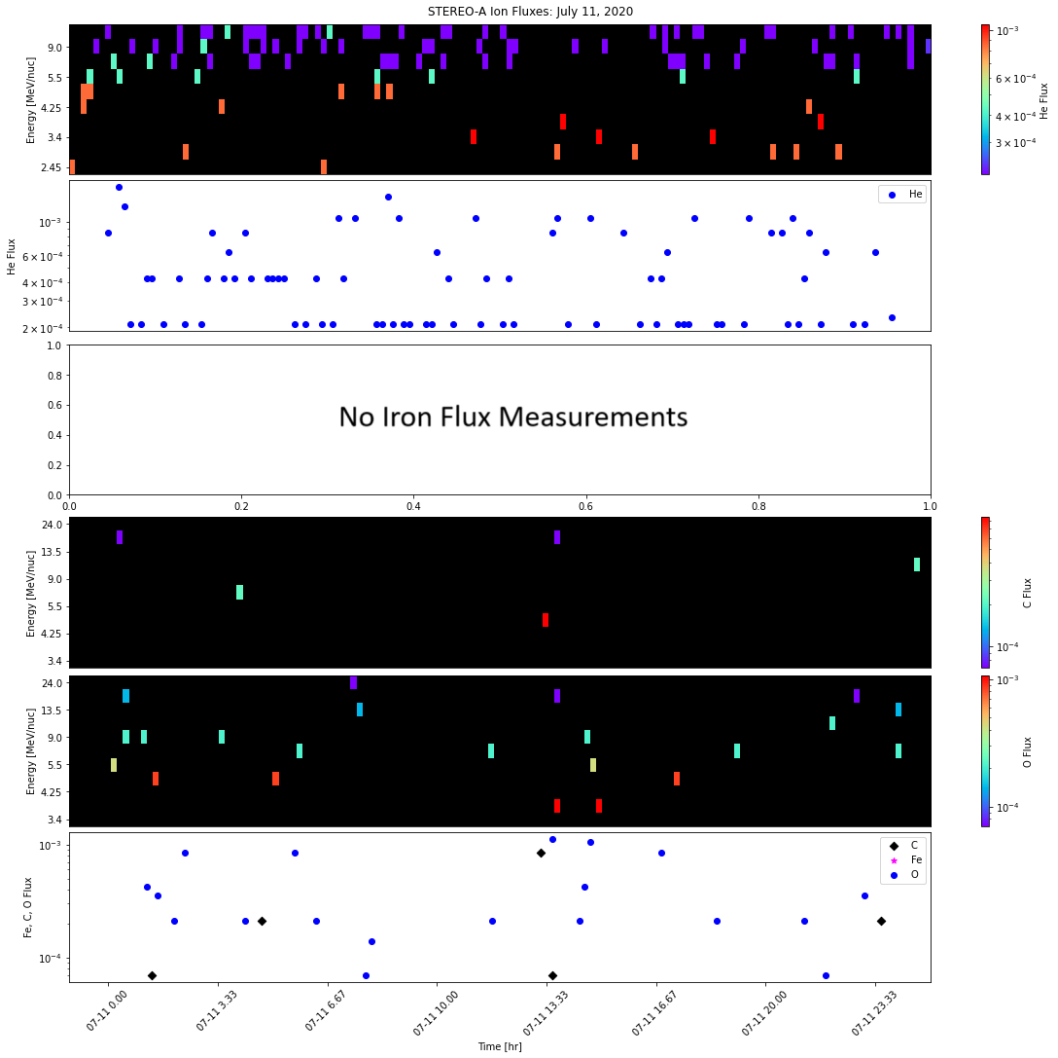

Figure 3.25: Event 4 (July 11, 2020) time analysis plots at STEREO-A.

STEREO-A was located almost 180°from SolO, and about 90°from PSP, so it is unlikely that STEREO-A would pick up this event. Figure 3.25 shows the time-analysis plots at STEREO-A, which do not show flux enhancements or time-dependent structure, indicating that STEREO-A did not see this event.

3.5 Event 5: July 20, 2020

The fifth event occurred on July 20, 2020. It was identified as a ^{3}He event by Solar Orbiter in Mason et al. (2021). Table 3.5 lists the distance from the sun, the start Carrington longitude, and the end Carrington longitude of each of the spacecraft during this event. During this event, the Parker Solar Probe was 0.79 AU from the sun while ACE and STEREO-A were about 1 AU from the sun. Solar Orbiter was

again closest to the sun at 0.67 AU.

Spacecraft	Distance From Sun [AU]	Start Carrington Longitude [°]	End Carrington Longitude [°]
PSP	0.79	318.9	305.5
ACE	1.02	297.4	284.3
STEREO-A	0.96	230.3	217.3
SolO	0.67	53.8	41.6

Table 3.5: Spacecraft distance from sun, and beginning and end Carrington Longitude during Event 5.

Figure 3.26 shows the positions of the spacecraft in relation to each other and to the sun and their nominal Parker spiral during this event. During this event SolO and PSP began 94.9°away from each other and ended 96.1°away from each other. SolO and ACE began 116.4°away from each other and ended 117.3°away from each other. SolO and STEREO-A began 183.8°away from each other and ended 184.3°away from each other. In this event, ACE and PSP's nominal parker spirals were very close together in during this event as well.

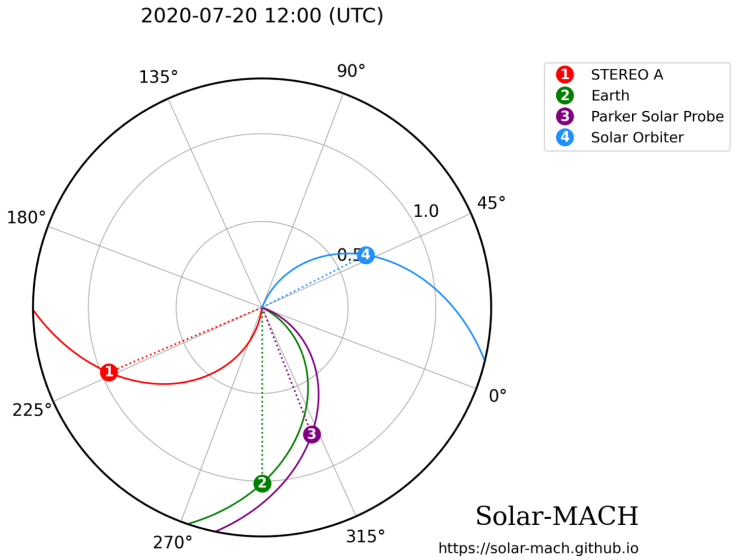

Figure 3.26: Positions of Spacecraft in relation to each other, the sun, and their nominal Parker spiral in the middle of Event 4. ACE orbits L1, so the position of the Earth is used to represent the position of ACE. Plot produced using Solar-MACH (Gieseler et al. 2022).

Time-Intensity Profile

Figures 3.27-3.29 are the time analysis plots for this event from PSP, ACE, and STEREO-A. Figures 3.27-3.29 are stacked time-analysis plots. These figures follow the same structure as the Figures in the other event sections.

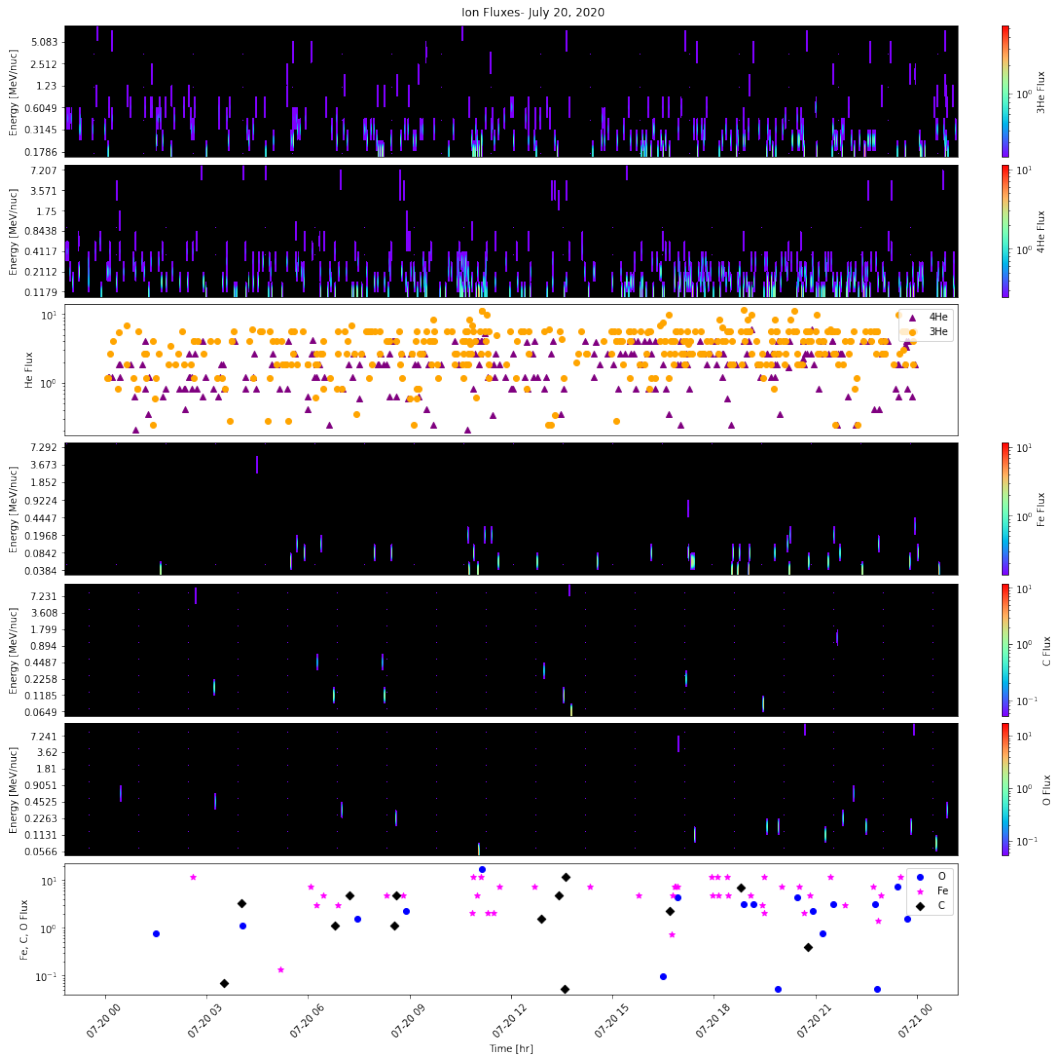

Figure 3.27: Event 5 (July 20, 2020) time analysis plots at SolO.

Figure 3.27 is the time-analysis stacked plot for event 5 at Solar Orbiter. There does not appear to be discernible a time-dependent structure in the time-intensity profiles or color bar plots for this event. There are enhanced flux measurements in ^{3}He, with a ^{3}He/^{4}He ratios reaching an order of magnitude of 10^0 at the onset of the event (expected ratio of an impulsive event) (Mason et al. 2021). Heavy Ion fluxes reach maximum values on the order of 10^1 cm^{-2} sr^{-1} sec^{-1} (keV/nuc)$^{-1}$. Like Event 5, ^{3}He and ^{4}He flux measurements appear to remain in the lower half of the SolO/EPD

(SIS) range.

PSP did not pick up this event. EPI-lo was either turned off to send data back to Earth, or there was an internal software malfunction, because the EPI-Lo CDF files for July 20, 2020 did not contain data. When EPI-hi was examined, there were only four measurements of flux for He, so no conclusions could be drawn from PSP during this event.

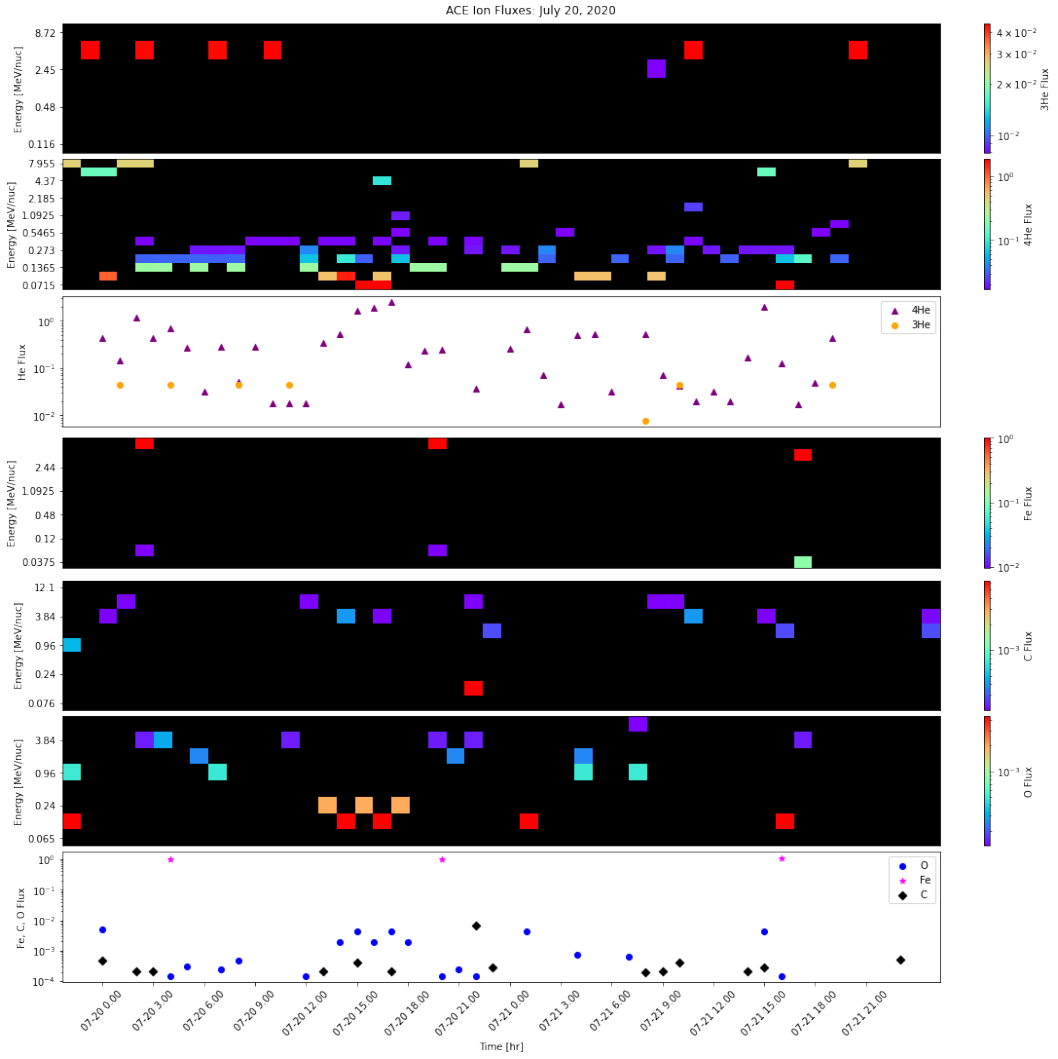

Figure 3.28: Event 5 (July 20, 2020) time analysis plots at ACE.

Figure 3.28 is the time-series analysis plots at ACE. ACE was located about 115°from SolO during this event. ^{3}He fluxes peak around 4x10^{-2} cm^{-2} sr^{-1} sec^{-1} (keV/nuc)$^{-1}$. Heavy Ion fluxes peak around the same value, with the exception of Iron which experiences a peak of about 10^0 cm^{-2} sr^{-1} sec^{-1} (keV/nuc)$^{-1}$. Although there are slightly increased fluxes of Fe, because ^{3}He flux values are barely above background,

and there is no obvious time-dependant structure, it is likely that ACE did not see this event.

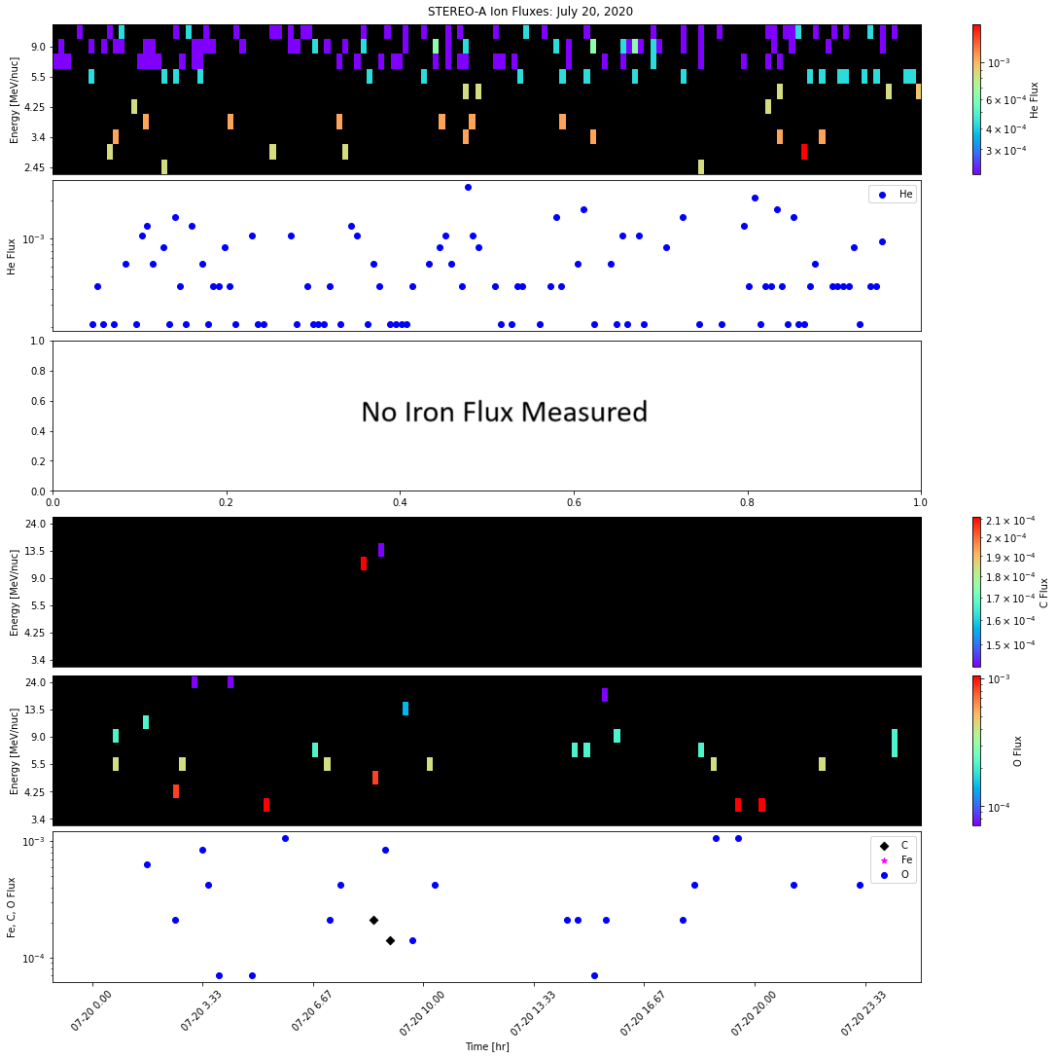

Figure 3.29: Event 5 (July 20, 2020) time analysis plots at STEREO-A.

Figure 3.29 is the time-series analysis plots at STEREO-A. STEREO-A was located around 180°from SolO during this event. He, C and O fluxes do not rise above background level, and no Fe measurements were taken at all. Because is no enhancement of He or the heavy ions, and no time-dependent structure, it is clear STEREO-A did not see this event.

3.6 Event 6: May 24-25, 2021

The sixth event occurred from May 24-25, 2021. It was identified as a particle enhancement in Mitchell et al. (2020). This event was not an impulsive event.

Figure 3.30 is a plot of the ^{3}He/^{4}He ratio during this event. This ratio is too small to be considered an impulsive event.

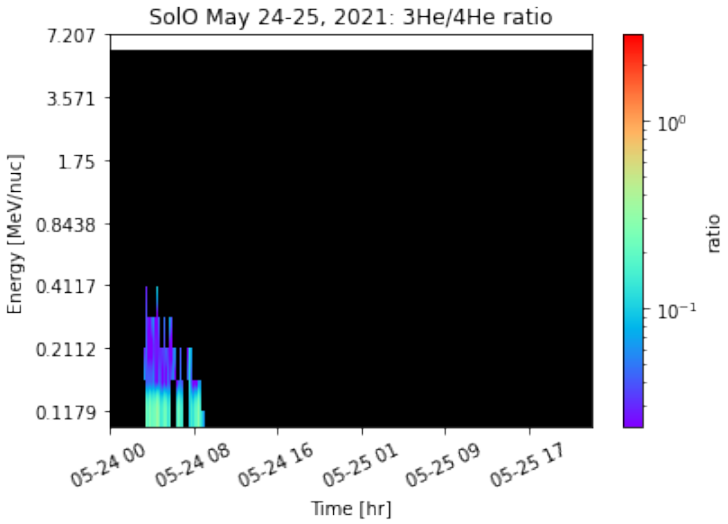

Figure 3.30: ^{3}He/^{4}He ratio during Event 6.

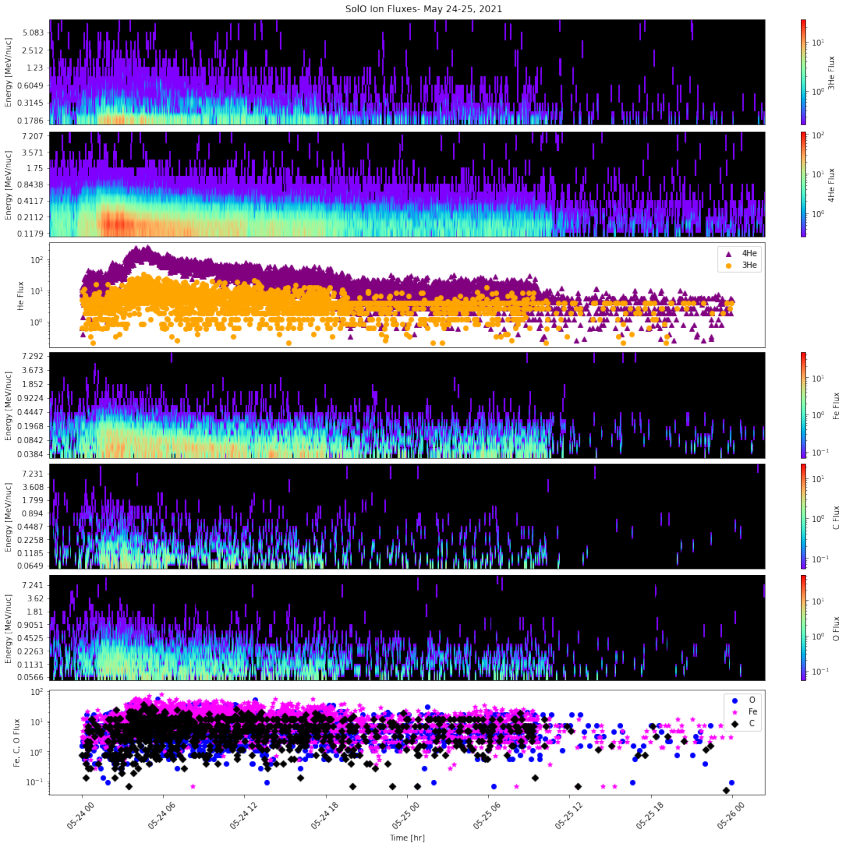

Figure 3.31: Event 6 (May 24-25, 2021) time analysis plots at SolO.

Furthermore, the time-intensity profile at SolO (Figure 3.31) better resembled the time-intensity profile of a gradual event, with a sharp peak at the onset of event then a slow decline. Finally, this event was identified and observed by PSP which was 159.9°away from SolO at the time of the event. ACE, which was between SolO and PSP also observed this event.

3.7 Spectra

Initial energetic ion spectra were gathered however, fitting to

$$J = J_0 E^{-\gamma} e^{\frac{E}{E_0}}$$

was difficult. Meaningful results could not be gathered in time to include in this thesis.

3.8 Event Overview

Event 1 and 2 came from the same active region, but had different particle populations (Event 1 had much more ^{3}He enhancements in the low energy range than Event 2). Event 2 was also the weaker of the pair (meaning it accelerated less ions to high energies (MeV) than Event 1 did). These events came from the same active region, but had very different heavy ion populations which may suggest a changing particle population on the sun. Event 1 was probably not observed by ACE, and it was not observed by STEREO-A. Event 2 was also not observed by ACE or STEREO-A.

The active region Event 3 initiated from is not known, but this event was observed by PSP and ACE which can help to constrain the longitudinal spread.

Events 4 was observed by Solar Orbiter in Mason et al. (2021) and by Parker Solar Probe in Mitchell et al. (2023), although more work need to be done to definitively constrain the longitudinal spread. Event 5 was both observed by Solar Orbiter in Mason et al. (2021) and was not observed by any other spacecraft (PSP did not collect data durring the event). The closest spacecraft collecting data during Event 5 was ACE, which did not see the event.

Event 6 was not an impulsive event. It's ^{3}He/^{4}He ratio was too low. However, it was observed by SolO, PSP, and ACE.

Chapter 4

DISCUSSION

4.1 Longitudinal Spread

Some events were easier to constrain than others. For events that were seen by two or more spacecraft or events with a known active region, constraining the longitudinal spread of an event was as simple as finding the angular separation between the spacecrafts or the location of the active region. However, may events had somewhat ambiguous results.

For Events 1 and 2, because active region 12,738 was not observed on one side, and Events 1 and 2 were observed by PSP which was separated by about 60°from the active region, they can be constrained to $> 60°$. Similarly, Event 3 was observed by PSP and ACE. ACE and PSP were separated by 60-65°over the length of this event, so depending on where the active region of this event was, the longitudinal spread of Event 3 may be constrained to less than or equal to 65°.

Events 4 and 5 are more ambiguous. It is possible that Event 4 was actually two separate, relatively narrow impulsive events that happened to go off in the same time period, or it's possible that SolO and PSP observed the same impulsive event. Determining the active region (s) that this event came from would be helpful in further constraining the longitudinal spread. Similarly determining the spectral index and cross-field diffusion coefficient would provide more context to how the particles are being accelerated and diffused through the heliosphere. Unfortunately, PSP did not have data for Event 5. Because ACE probably did not see this event and it is unknown if PSP would have, it is hard to constrain the longitudinal spread, although it was probably less than 115°. Finally, although Event 6 was not an impulsive event, although it's longitudinal spread can be constrained to a least 160°. Events 1-3 most likely had longitudinal spreads close to 60°, which is consistent with the majority of impulsive events. It is difficult to definitively constrain the spreads of Events 4 and 5.

4.2 Cross-field Diffusion and Future Work

Significant cross-field diffusion could have contributed to any of the spreads of the impulsive events, but without modeling efforts nothing definitive can be said about

the cross-field diffusion.

The particle populations in the events, particularly in the first two events reveal a little bit about the particle populations on the sun at the on set of the events. Using the energetic ion spectra, more insight can be gained to the initial conditions of an event.

More information about how particles are being accelerated from flare sites can be obtained by finding the spectral index of the energetic ion spectra of these events. This, and the cross-field diffusion coefficient will help further constrain the longitudinal spread of these events. Fitting the energetic ion spectra is within the scope of the work and will be continued, however, finding the cross-field diffusion coefficient would require modeling the events.

BIBLIOGRAPHY

ACE Mission. izw1caltechedu. https://izw1.caltech.edu/ACE/ace_mission.html.

Bruno A, Christian ER, Nolfo GA, Richardson IG, Ryan JM. 2019. Spectral Analysis of the September 2017 Solar Energetic Particle Events. Space Weather. 17(3):419–437. doi:https://doi.org/10.1029/2018sw002085.

Costa Jr. E da, Tsurutani BT, Alves MV, Echer E, Lakhina GS. 2013. CROSS-FIELD DIFFUSION OF ENERGETIC (100 keV to 2 MeV) PROTONS IN INTERPLANETARY SPACE. Astrophysical Journal/The Astrophysical Journal. 778(2):180–180. doi:https://doi.org/10.1088/0004-637x/778/2/180.

Desai M, Giacalone J. 2016. Large gradual solar energetic particle events. Living Reviews in Solar Physics. 13(1). doi:https://doi.org/10.1007/s41116-016-0002-5.

Espinosa Lara F. 2022. SOLAR ORBITER ENERGETIC PARTICLE DETECTOR EPD DATA PRODUCT DESCRIPTION DOCUMENT. Rodriguez-Pacheco J, editor. (1).

European Space Agency. Solar Orbiter overview. wwwesaint. https://www.esa.int/Science_Exploration/Space_Science/Solar_Orbiter_overview.

European Space Agency. Solar Orbiter Instruments. wwwesaint. https://www.esa.int/ESA_Multimedia/Images/2020/01/Solar_Orbiter_Instruments.

Fletcher L, Dennis BR, Hudson HS, Krucker S, Phillips K, Veronig A, Battaglia M, Bone L, Caspi A, Chen Q, et al. 2011. An Observational Overview of Solar Flares. Space Science Reviews. 159(1):19. doi:https://doi.org/10.1007/s11214-010-9701-8. https://link.springer.com/article/10.1007%2Fs11214-010-9701-8.

Gieseler, J., Dresing, N., Palmroos, C., von Forstner, J.L.F., Price, D.J., Vainio, R. et al. (2022). Solar-MACH: An open-source tool to analyze solar magnetic connection configurations. *Front. Astronomy Space Sci.* 9. doi:10.3389/fspas.2022.1058810

Laitinen T, Dalla S, Marsh MS. 2013. ENERGETIC PARTICLE CROSS-FIELD PROPAGATION EARLY IN A SOLAR EVENT. The astrophysical journal Letters. 773(2):L29–L29. doi:https://doi.org/10.1088/2041-8205/773/2/l29.

Leske RA, Christian ER, Cohen S, Cummings AC, Davis A, Desai MM, Giacalone J, Hill M, Joyce CJ, Krimigis SM, et al. 2019. Observations of the 2019 April 4 Solar Energetic Particle Event at the *Parker Solar Probe*. The Astrophysical Journal Supplement Series . 246(2):35–35. doi:https://doi.org/10.3847/1538-4365/ab5712.

Li G, Jin M, Ding Z, Bruno A, de Nolfo GA, Randol BM, Mays L, Ryan J, Lario D. 2021. Modeling the 2012 May 17 Solar Energetic Particle Event Using the AWSoM and iPATH Models. The Astrophysical Journal. 919(2):146. doi:https://doi.org/10.3847/1538-4357/ac0db9.

Liu Z, Wang L, Wimmer-Schweingruber RF, Krucker S, Mason GM. 2020. Pan-Spectrum Fitting Formula for Suprathermal Particles. Journal of Geophysical Research: Space Physics. 125(12). doi:https://doi.org/10.1029/2020ja028702.

Malandraki OE, Crosby NB. 2018. Solar Particle Radiation Storms Forecasting and Analysis. Springer.

Malandraki OE, Cohen S, Giacalone J, Mitchell JG, R. Chhiber, McComas DJ, J. Rodríguez-Pacheco, Wimmer-Schweingruber RF, Ho GC. 2023. Unexpected energetic particle observations near the Sun by Parker Solar Probe and Solar Orbiter. Physics of plasmas. 30(5). doi:https://doi.org/10.1063/5.0147683.

Mason GM, Gold RE, Krimigis SM, Mazur JE, Andrews GB, Daley KA, Dwyer JR, Heuerman K, James T, Kennedy M, et al. 1998. The Ultra-Low-Energy Isotope Spectrometer (ULEIS) for the ACE spacecraft. Space Science Reviews. 86(1/4):409–448. doi:https://doi.org/10.1023/a:1005079930780.

Mason GM, Ho GC, Allen RC, Rodríguez-Pacheco J, Wimmer-Schweingruber RF, Bučík R, Gómez-Herrero R, Lario D, Forstner von, Andrews GB, et al. 2021. ^{3}He-rich solar energetic particle events observed on the first perihelion pass of Solar Orbiter. Astronomy and Astrophysics. 656:L1–L1. doi:https://doi.org/10.1051/0004-6361/202039752.

McComas DJ, Alexander N, Angold N, Bale S, Beebe C, Birdwell B, Boyle M, Burgum JM, Burnham JA, Christian ER, et al. 2014. Integrated Science Investigation of the Sun (ISIS): Design of the Energetic Particle Investigation. Space Science Reviews. 204(1-4):187–256. doi:https://doi.org/10.1007/s11214-014-0059-1.

McComas DJ, Christian ER, Cohen CMS, Cummings AC, Davis AJ, Desai MI, Giacalone J, Hill ME, Joyce CJ, Krimigis SM, et al. 2019. Probing the energetic particle environment near the Sun. Nature. 576(7786):223–227. doi:https://doi.org/10.1038/s41586-019-1811-1.

Mewaldt RA, Cohen S, Cook WR, Cummings AC, Davis A, Geier S, B. Kecman, J. Klemic, Labrador AW, Leske RA, et al. 2008. The Low-Energy Telescope (LET) and SEP Central Electronics for the STEREO Mission. Space Science Reviews. 136(1-4):285–362. doi:https://doi.org/10.1007/s11214-007-9288-x.

Mitchell JG, Cohen S, Eddy TJ, Joyce CJ, Rankin JS, Shen MM, de A, Christian ER, McComas DJ, McNutt RL, et al. 2023. A Living Catalog of Parker Solar Probe IS⊙IS Energetic Particle Enhancements. The Astrophysical Journal Supplement Series. 264(2):31–31. doi:https://doi.org/10.3847/1538-4365/aca4c8.

NASA. 2018 Aug 12. Parker Solar Probe - NASA Science. sciencenasagov. https://science.nasa.gov/mission/parker-solar-probe/.

NASA. ACE - NASA Science. sciencenasagov. https://science.nasa.gov/mission/ace/.

Nasa C, Johns, Apl H, Gribben S. Parker Solar Probe A Mission to Touch the Sun. https://www.nasa.gov/wp-content/uploads/2018/02/parkersolarprobe_presskit_august2018_final.pdf?emrc=0e3e48

NASA. STEREO. stereogsfcnasagov. https://stereo.gsfc.nasa.gov/mission/mission.shtml.

Parker EN. 1958. Dynamics of the Interplanetary Gas and Magnetic Fields. The Astrophysical Journal. 128:664. doi:https://doi.org/10.1086/146579. http://articles.adsabs.harvard.edu/cgi-bin/nph-iarticle_query?1958ApJ...128..664P&data_type=PDF_HIGH&whole_paper=YES&type=PRINTER&filetype=.pdf.

Poduval B, Niehof J, de Wet W. PSP/IS⊙IS Energetic Particle Data - User Guide.

Reames DV. 2021. Solar Energetic Particles. Springer Nature.

Reames DV. 2023. Review and outlook of solar energetic particle measurements on multispacecraft missions. Frontiers in astronomy and space sciences. 10. doi:https://doi.org/10.3389/fspas.2023.1254266.

Rodríguez-Pacheco J, Wimmer-Schweingruber RF, Mason GM, Ho GC, Sánchez-Prieto S, Prieto M, Martín C, Seifert H, Andrews GB, Kulkarni SR, et al. 2020. The Energetic Particle Detector - Energetic particle instrument suite for the Solar Orbiter mission. Astronomy & Astrophysics. 642:A7. doi:https://doi.org/10.1051/0004-6361/201935287. https://www.aanda.org/articles/aa/full_html/2020/10/aa35287-19/aa35287-19.html.

Tsurutani BT. 2003. The extreme magnetic storm of 1–2 September 1859. Journal of Geophysical Research. 108(A7). doi:https://doi.org/10.1029/2002ja009504.

Wiedenbeck ME, Mason GM, Cohen S, Nitta NV, Gómez-Herrero R, Haggerty DK. 2012. OBSERVATIONS OF SOLAR ENERGETIC PARTICLES FROM^{3}He-RICH EVENTS OVER A WIDE RANGE OF HELIOGRAPHIC LONGITUDE. The Astrophysical Journal. 762(1):54–54. doi:https://doi.org/10.1088/0004-637x/762/1/54.

Wiedenbeck ME, R. Bučík, Mason GM, Ho GC, Leske RA, Cohen S, Christian ER, Cummings AC, Davis AJ, Desai MI, et al. 2020. ^{3}He-rich Solar Energetic Particle Observations at the *Parker Solar Probe* and near Earth. The Astrophysical journal Supplement series/Astrophysical journal Supplement series. 246(2):42–42. doi:https://doi.org/10.3847/1538-4365/ab5963.